

## Geological Society of America Bulletin

### Episodic arc migration, crustal thickening, subduction erosion, and magmatism in the south-central Andes

Suzanne Mahlburg Kay, Estanislao Godoy and Andrew Kurtz

*Geological Society of America Bulletin* 2005;117, no. 1-2;67-88  
doi: 10.1130/B25431.1

---

#### Email alerting services

click [www.gsapubs.org/cgi/alerts](http://www.gsapubs.org/cgi/alerts) to receive free e-mail alerts when new articles cite this article

#### Subscribe

click [www.gsapubs.org/subscriptions/](http://www.gsapubs.org/subscriptions/) to subscribe to Geological Society of America Bulletin

#### Permission request

click <http://www.geosociety.org/pubs/copyrt.htm#gsa> to contact GSA

Copyright not claimed on content prepared wholly by U.S. government employees within scope of their employment. Individual scientists are hereby granted permission, without fees or further requests to GSA, to use a single figure, a single table, and/or a brief paragraph of text in subsequent works and to make unlimited copies of items in GSA's journals for noncommercial use in classrooms to further education and science. This file may not be posted to any Web site, but authors may post the abstracts only of their articles on their own or their organization's Web site providing the posting includes a reference to the article's full citation. GSA provides this and other forums for the presentation of diverse opinions and positions by scientists worldwide, regardless of their race, citizenship, gender, religion, or political viewpoint. Opinions presented in this publication do not reflect official positions of the Society.

---

#### Notes

# Episodic arc migration, crustal thickening, subduction erosion, and magmatism in the south-central Andes

Suzanne Mahlburg Kay<sup>†</sup>

*INSTOC, Snee Hall, Cornell University, Ithaca, New York 14853, USA*

Estanislao Godoy<sup>‡</sup>

*SERNAGEOMIN, Casilla 10465, Santiago, Chile*

Andrew Kurtz<sup>§</sup>

*Department of Earth Sciences, Boston University, Boston, Massachusetts 02215, USA*

## ABSTRACT

The past ~25 m.y. of geologic history in the northern ~300 km (~33°–36°S) of the Andean Southern Volcanic Zone has seen waxing and waning magmatic production rates and episodic eastward relocation of arc segments accompanied by abrupt chemical changes in the magmas. These changes can be linked to episodes of crustal thickening at times of backarc thrusting and to peaks of subduction erosion of forearc crust and mantle lithosphere at times of frontal-arc migration to the east. The magmatic-tectonic coupling is well seen in the history—enhanced by 28 new K-Ar ages, >160 major and trace element analyses, and Sr, Nd, and Pb isotope analyses—of a west to east transect through the El Teniente copper district near 34°S. The temporal trends in magmatic chemistry in this transect are like the well-documented south to north trends in Pleistocene to Holocene volcanic centers of the Southern Volcanic Zone, and both can be linked to the same events. The magmatic changes require differences in magma source regions as shown by isotopic data and in depths of crustal magma generation/fractionation as shown by pressure-sensitive trace element distributions. “Adakitic” magmas in the region are attributed to a combination of melting the base of thickened lower crust and crust entering the mantle through subduction erosion. Subduction erosion is argued to peak in episodes of frontal-arc migration at ca. 19–16 Ma and ca. 7–4 Ma. The combined effects of crustal shortening and forearc truncation in the

past 20 m.y. near 34°S have led to the loss of ~170 km of crustal width. The timing and arc length over which these events occurred show that subduction of the Juan Fernández Ridge on the Nazca plate cannot have been the major driving force. The history of the region shows the importance of non-steady-state processes in arc-magma production and the necessity of studying arc systems over millions, not tens of thousands, of years.

**Keywords:** Andes, Southern Volcanic Zone, magmatism, subduction erosion, thick crust, geochemistry, isotopes, Miocene.

## INTRODUCTION

The Andean Southern Volcanic Zone (SVZ, Fig. 1) with its relatively simple subduction geometry, nearly constant arc-trench gap, and systematic along-strike chemical changes has been the subject of a series of classical studies aimed at understanding the relationship of Pleistocene to Holocene SVZ magmas to continental-margin tectonics (e.g., López-Escobar et al., 1977; Hickey et al., 1986; Futa and Stern, 1988; Hildreth and Moorbath, 1988; Stern, 1991; Tormey et al., 1991, 1995; Dungan et al., 2001). The pronounced south to north chemical variations identified in these magmas have been attributed to increasing crustal thickness and changing lithology and age of arc basement (e.g., Hildreth and Moorbath, 1988) and/or to variable contributions from subducted sediment and crust added to the mantle wedge by subduction erosion (Stern, 1991). Differences in percentage of mantle melting have also been argued to play a role (e.g., López-Escobar et al., 1977; Tormey et al., 1991; Stern, 1991). A general consensus has not been reached on the relative importance of these processes, as sources of

continental crustal contaminants are difficult to differentiate on geochemical grounds.

The role of forearc subduction erosion—the process in which crust is plucked or abraded from the hanging wall above the subducting slab and dragged down under the arc where it could become a component in arc magmas—has long been debated along the Chilean margin (e.g., Rutland, 1971; von Huene and Scholl, 1991; Stern, 1991). Evidence for subduction erosion comes from map patterns of Paleozoic and Mesozoic rocks (Fig. 1) that suggest that over several hundred million years, continental crust has been removed from along the Chilean coast. Quantitatively, the removal rate has been argued to be comparable to that of arc-magma production and sediment subduction (e.g., von Huene and Scholl, 1991). What has been less clear is when subduction erosion occurred, whether the process is continuous or episodic, and whether crustal and lithospheric mantle components from subduction erosion actually make their way into arc-magma sources.

Relevant to debates on the sources of SVZ arc magmas and the roles of subduction erosion and crustal thickening are early Miocene to Holocene magmatic changes along the margin. These temporal changes have been little addressed as only scanty chemical data have been available on Tertiary magmatic rocks beneath and west of the SVZ. Geochemical studies have been impeded by widespread moderate to severe secondary hydrothermal alteration and uncertainties about the ages of the magmatic rocks (e.g., Vergara et al., 1988). With the exception of a few, mostly reconnaissance studies (e.g., López-Escobar et al., 1997; Vergara et al., 1999; Yáñez et al., 2002), available chemical and isotopic data have been from host rocks of the giant copper deposits between 32°S and 34°S (Pelambres-Pachon,

<sup>†</sup>E-mail: [smk16@cornell.edu](mailto:smk16@cornell.edu).

<sup>‡</sup>E-mail: [egodoy@sernageomin.cl](mailto:egodoy@sernageomin.cl).

<sup>§</sup>E-mail: [kurtz@bu.edu](mailto:kurtz@bu.edu).

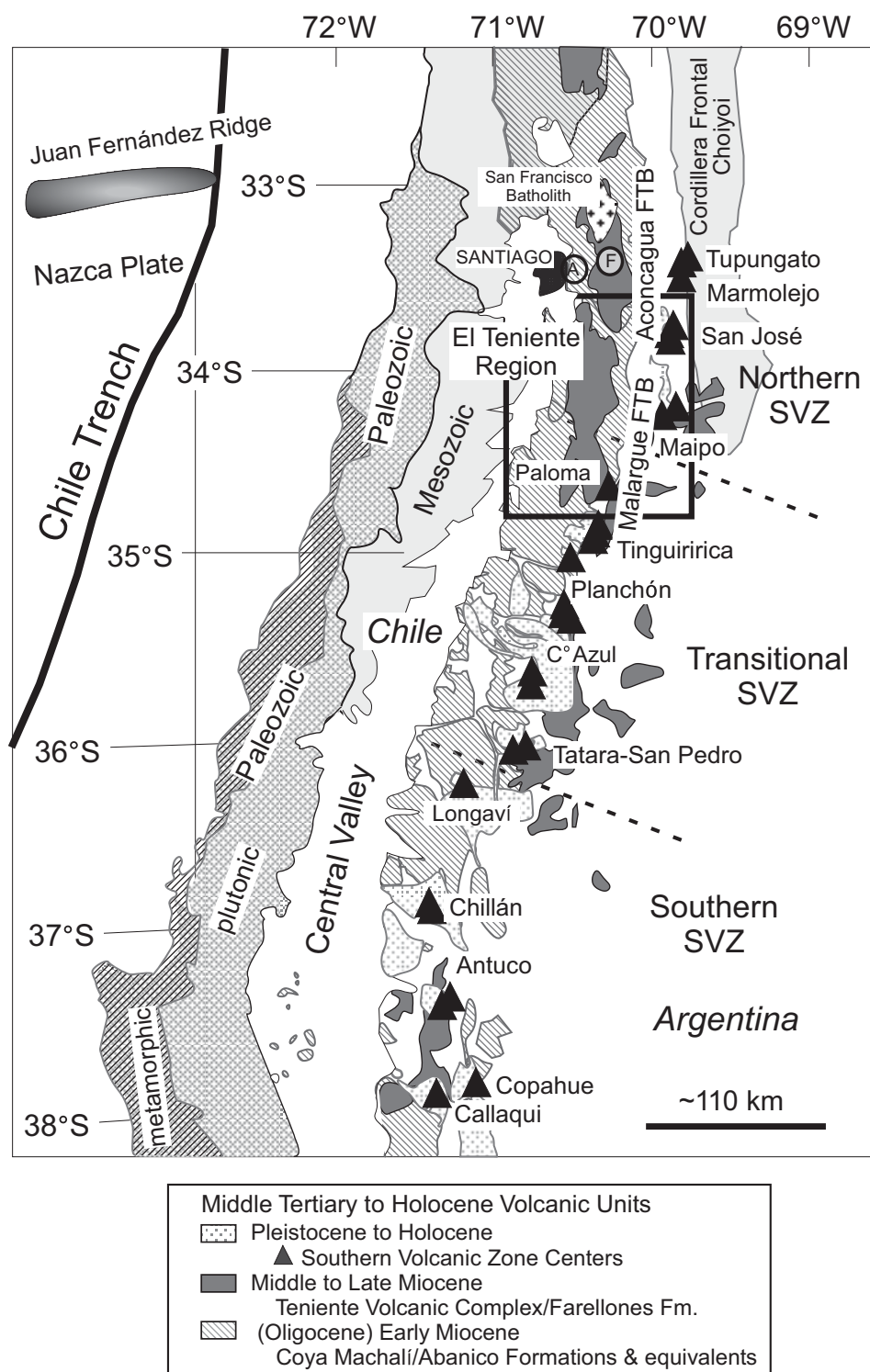


**Figure 1.** Map of Andes from north of lat 33°S to lat 38°S showing distribution of late Oligocene/early Miocene and middle to late Miocene magmatic units, the SVZ volcanic centers, the generalized extent of forearc Paleozoic and Mesozoic (mainly Cretaceous) outcrops, the Frontal Cordillera where the upper Paleozoic to lower Mesozoic Choiyoi Group is exposed, and the locations of the backarc Aconcagua and Malargue fold-thrust belts (FTB). Offsets in the modern volcanic line are marked by the northwest-trending dashed lines at ~36.2°S and 34.5°S that separate the SVZ into the northern SVZ, transitional SVZ (Paloma to Tatara-San Pedro), and southern SVZ segments. The El Teniente region within the heavy lined box is shown in more detail in Figure 2. The city of Santiago, the Central Valley, the Chile Trench, and the Juan Fernández Ridge are shown for reference. Circles labeled A and F near Santiago are locations of the Abanico and Farellones Formation samples discussed in the text. Map is based on the 1:1,000,000 scale geologic map of Chile (Servicio Nacional de Geología y Minería, Santiago, Chile, 1980) and the 1:2,500,000 scale geologic map of Argentina (Servicio Geológico Minero Argentino, Buenos Aires, Argentina, 1997).

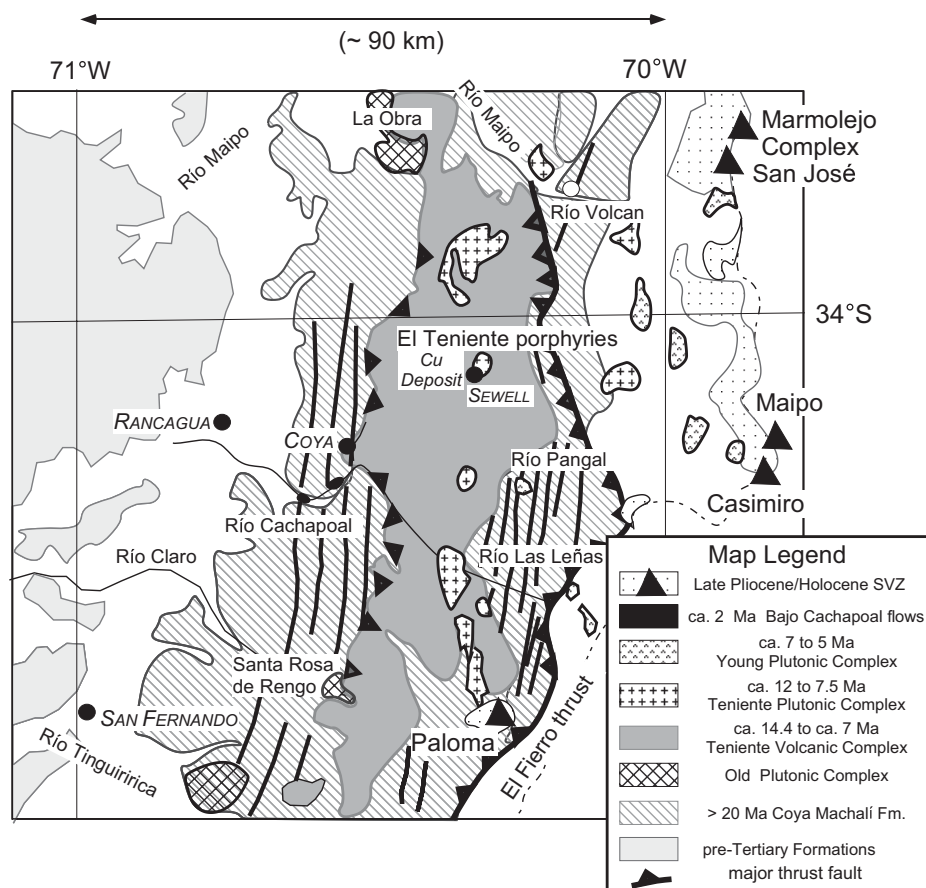


**Figure 2.** Map showing the distribution of early Miocene to Holocene magmatic units and principal structural features in the El Teniente region (box in Fig. 1). La Obra and Santa Rosa de Rengo are names of plutons in the Old Plutonic Complex, El Fierro thrust is out-of-sequence thrust discussed in text, and north-trending lines are traces of other major thrust faults and fold axis. The El Teniente copper deposit is associated with the El Teniente porphyries. Principal towns marked by dark circles (names in *italics*; El Teniente mine is at Sewell) and rivers shown for reference. Map is modified from geologic maps of Charrier et al. (1996), and Godoy et al. (1999). See text for discussion. SVZ—Southern Volcanic Zone.

Los Bronces, and El Teniente; e.g., Camus, 1975; Skewes and Stern, 1994, 1995, 1996; Kay et al., 1999; Kay and Mpodozis, 2001, 2002; Skewes et al., 2002).

In this light, the purpose of this paper is threefold. The first is to present extensive new K-Ar ages and whole-rock chemical and isotopic data for early Miocene to Pliocene arc rocks in a transect of the SVZ forearc near 34°S (El Teniente transect; Figs. 1 and 2). The second is to define and interpret the chemical and isotopic trends in these data in the framework of an ~25 m.y. tectonic interval. The case is made that crustal contaminants entering these magmas are linked to both crustal thickening and forearc subduction erosion (e.g., von Huene and Scholl, 1991); the former peaked as the crust thickened in response to crustal shortening, and the latter peaked during times of frontal-arc migration

to the east. The process of forearc subduction erosion is argued to be compatible with sudden and transient geochemical changes in these magmas. The third is to argue that south to north chemical trends along the SVZ that parallel early Miocene to Holocene trends in the El Teniente transect reflect the same crustal-thickening and arc-migration events. The results have implications for the evolution of Andean-type margins elsewhere (e.g., Sierra Nevada, Canadian Cordillera) and for discussions of mass fluxes along continental margins.

#### TECTONIC SETTING AND MAGMATIC UNITS IN THE EL TENIENTE TRANSECT

The early Miocene to Pliocene magmatic arc rocks of the El Teniente transect sit between

33°55'S and 34°20'S in the forearc of the SVZ (Figs. 1 and 2). This part of the SVZ, commonly called the northern SVZ segment, lies between the volcanically inactive Chilean flat-slab region (28°S–33°S) that overlies a nearly horizontal part of the subducting Nazca plate to the north (e.g., Cahill and Isacks, 1992) and an offset in the SVZ near 34.5°S. The northern SVZ to Chilean flat-slab boundary projects offshore toward the Juan Fernández Ridge (Fig. 1) whose intersection with the Chile trench has migrated southward. The subduction of this ridge has been argued by Yáñez et al. (2002), among others, to have been responsible for the Miocene shallowing of the subducting plate under the Chilean flat-slab (Kay et al., 1987) and incipient shallowing under the northern SVZ. The rest of the SVZ, south of 34.5°S, can be divided into the transitional SVZ and the southern SVZ, whose boundary is commonly put at the offset in the volcanic line near 35.2°S. The northern SVZ is distinct from the transitional SVZ and southern SVZ in being underlain by a thick crust (up to ~60–65 km); the crust thins progressively to ~35 km in the southern SVZ (e.g., Introcaso et al., 1992). Volcanoes in the northern SVZ are ~100 km above the seismic zone in the subducting slab, whereas those farther south are at ~115 km (Cahill and Isacks, 1992; Pardo et al., 2002).

A summary of the early Miocene to Holocene magmatic rocks in the El Teniente transect and a regional deformational history are shown in Table 1. A regional map based on maps in Godoy (1993), Charrier et al. (1996), and Godoy et al. (1999) is shown in Figure 2. The ages and regional setting of the El Teniente transect magmatic rocks are discussed below, and their chemistry is covered in the next section. Their emplacement ages have a history of controversy owing to uncertainties over resetting of K-Ar ages by younger magmatic events (e.g., Vergara et al., 1988; Charrier and Munizaga, 1979; Charrier et al., 1996). The acceptance of late Oligocene to Pliocene ages for all of them has been relatively recent (Godoy, 1993; Kay et al., 1999; Charrier et al., 1996, 2002) and has been influenced by the 28 previously unpublished K/Ar ages in Table 2. Geologic mapping of the region has been complicated by difficulties in identifying eruptive centers in eroded, altered volcanic rocks as well as areas of steep topography with frequent landslides. Similar problems throughout this region of the Andes have resulted in the volcanic rocks of this age being traditionally assigned to the older, more deformed, altered, and sediment-rich Abanico Formation and the younger Farellones Formation (e.g., Vergara et al., 1988).

TABLE 1. MAGMATIC AND STRUCTURAL SUMMARY FOR EL TENIENTE REGION/NORTHERN SOUTHERN VOLCANIC ZONE TRANSECT

Magmatic group and age (Ma)	Magmatic units/deformational events	Magmatic conditions
<b>1</b> Figure 9F <2	Northern Southern Volcanic Zone (SVZ) centers	High pressure
<b>2</b> ca. 2.3–1.8 3.8–2.8 ca. 5.5–4.5 Figure 9E ca. 7–5	Bajo Cachapoal lavas in modern SVZ forearc Late Hornblende Dike group Thrusting near magmatic front ends by 5.7 Ma, continues in distal backarc El Teniente related porphyries Young Plutonic Complex EASTWARD FRONTAL-ARC MIGRATION: ~50 km	High pressure High pressure, relatively dry Garnet rich, feldspar poor
<b>3</b> Figure 9D ca. 8.5–5? ca. 9–7 ca. 9.3–6.5 ca. 9 Figure 9C ca. 10.7–9.9 Figure 9B ca. 14–10.6 ca. 13–11 ca. 14.4–11.5 15.7	Uplift, compressional inversion, thrusting (out-of-sequence) in arc region Younger part of Teniente Plutonic Complex Teniente Volcanic Complex Upper Sewell Group† Thick-skinned uplift of Frontal Cordillera Range in backarc Teniente Volcanic Complex Lower Sewell Group† Thrusting (in-sequence) in backarc Aconcagua and Marlague fold-thrust belts Older part of Teniente Plutonic Complex Teniente Volcanic Complex Maqui Chico Group† Old Plutonic Complex—Santa Rosa de Rengo pluton EASTWARD FRONTAL ARC MIGRATION: ~35 km Uplift, compressional inversion of older normal faults	Medium to high pressure amp, plag, minor cpx Medium pressure, wet cpx, amp, plag Medium pressure, wet, oxidizing cpx, amp, plag, titanite
<b>4</b> Figure 9A ca. 20–19 ca. 27–20 31?–16 ?	Old Plutonic Complex—La Obra pluton Western belt—Coya Machalí Formation‡ Eastern belt—Coya Machalí Formation‡	Low pressure, dry ol, opx, cpx plag

Note: See text for references; amp—amphibole, plag—plagioclase, cpx—clinopyroxene, opx—orthopyroxene, ol—olivine.  
†Mapped regionally as the Farellones Formation.  
‡Mapped regionally as the Abanico Formation.

## Early Miocene: Arc Magmatism in a Noncontractional Regime

The oldest group in Table 1 includes the Abanico Formation, which is mapped in the El Teniente transect as the Coya Machalí Formation (Charrier et al., 1996, 2002), and the Old Plutonic Complex (Kurtz et al., 1997). Together, they formed in the Oligocene–early Miocene magmatic arc (Figs. 1 and 2).

The Coya Machalí Formation is a voluminous basaltic to rhyolitic volcanic and sedimentary complex composed of volcanic flows, agglomerates, lithic tuffs, and volcanoclastic and lacustrine sediments cut by dikes. Stratigraphic thicknesses are locally up to 1300 m. Regionally, the outcrops occur in a volcanic rock–rich western belt and a sedimentary rock–rich eastern belt (Fig. 2). The age of the western belt is constrained by K/Ar dates that range from 27.7 Ma to 20.5 Ma (Charrier et al., 1996, 2002)

and the  $27.7 \pm 2$  Ma date on an andesite dike in Table 2. These ages are consistent with K/Ar and  $^{40}\text{Ar}/^{39}\text{Ar}$  dates that range from  $26 \pm 1.2$  to  $18.8 \pm 0.8$  Ma in the Abanico Formation near Santiago (Fig. 1; see Gana et al., 1999). The age of the eastern belt is considered to be Oligocene to early Miocene based on K–Ar ages between ca. 37 Ma (Charrier et al., 2002) and  $16.1 \pm 0.5$  Ma (Kay et al., 1999) and on mammalian fossils (Charrier et al., 1996, 2002). All of these rocks have been subjected to low-temperature metamorphism and post–early Miocene folding and faulting (e.g., Charrier et al., 1996; Godoy et al., 1999).

The Old Plutonic Complex includes the plutons that cut the western belt of the Coya Machalí Formation (Fig. 2; López-Escobar et al., 1979; Kurtz et al., 1997). The age of the La Obra leucogranodiorite is constrained by an  $^{40}\text{Ar}/^{39}\text{Ar}$  biotite age of  $19.6 \pm 0.5$  Ma (Kurtz et al., 1997).

## Latest Early to Earliest Middle Miocene: Near Lull in Magmatism in a Contractional Regime

Except for the Santa Rosa de Rengo pluton (Fig. 2) with a hornblende  $^{40}\text{Ar}/^{39}\text{Ar}$  age of  $16.2 \pm 1.2$  Ma (Kurtz et al., 1997) and a small intrusion with a K/Ar age of  $15.2 \pm 1.2$  Ma (Table 2), 19.6–15 Ma magmatic rocks are unknown in the El Teniente transect. Farther north, K/Ar ages from 21.6 to 16.6 Ma are reported in Farellones Formation volcanic sequences east of Santiago (Fig. 1; Beccar et al., 1986; Aguirre et al., 2000). This period is that of the relatively high exhumation rate for (1) the La Obra pluton ( $\sim 0.55$  mm/yr) as proposed by Kurtz et al. (1997) on the basis of  $^{40}\text{Ar}/^{39}\text{Ar}$  biotite ( $19.6 \pm 0.5$  Ma) and K-feldspar ( $16.2 \pm 0.3$  Ma) ages, and (2) the San Francisco pluton northeast of Santiago (Fig. 1) based on mineral K/Ar ages (Warnaars et al., 1985; Serrano et al., 1996). Godoy et al.



TABLE 2. K/Ar RADIOMETRIC AGES FOR EL TENIENTE TRANSECT SAMPLES

Sample	Rock type	Latitude (UTM grid)	Longitude (UTM grid)	type	K (%)	Ar radiogenic (nL/g)	Ar atmospheric (%)	Age (Ma)
<u>Coya Machalí Formation</u>								
E2635	Andesite dike	6113.30	377.75	whole rock	0.345	0.375	69	27.7 ± 2.0
<u>Farellones Formation</u>								
Tte-93	Two-pyroxene andesite	6207.25	359.80	whole rock	0.825	0.491	71	15.2 ± 1.2
<u>Teniente Volcanic Complex—Maqui Chico Group</u>								
KET-1	Two-pyroxene andesite	6232.30	368.45	whole rock	1.777	0.973	72	14.0 ± 0.9
KET-16	Quartz diorite dike	6242.00	366.28	whole rock	1.745	0.949	57	13.9 ± 0.7
KET-25	Hornblende andesite	6233.92	363.80	whole rock	2.336	1.117	55	12.3 ± 0.5
Tte-143	Hornblende dacite breccia	6234.04	365.40	hornblende	0.467	0.218	88	12.0 ± 2.2
E-2695	Clinopyroxene andesite	6225.34	365.61	whole rock	1.401	0.658	59	12.0 ± 0.7
MIN-3	Andesite bomb	6225.93	364.65	whole rock	3.094	1.375	45	11.4 ± 0.4
<u>Teniente Volcanic Complex—Lower Sewell Group</u>								
E-2689	Clinopyroxene andesite	6225.30	365.79	whole rock	2.206	0.924	46	10.7 ± 0.5
Ket-154	Clinopyroxene andesite	6215.45	373.00	whole rock	0.925	0.378	50	10.5 ± 0.8
Ket-147	Clinopyroxene andesite	6215.30	368.65	whole rock	1.896	0.774	34	10.5 ± 0.4
Ket-157A	Clinopyroxene andesite	6215.45	373.00	whole rock	0.990	0.397	67	10.3 ± 0.8
Ket-92-3	Clinopyroxene andesite	6232.30	368.45	whole rock	1.614	0.636	75	10.1 ± 0.8
Ket-29	Andesite sill	6231.64	364.72	whole rock	3.282	1.271	64	9.9 ± 0.5
<u>Teniente Volcanic Complex—Upper Sewell Group</u>								
E-2797	Welded tuff	6226.43	362.25	whole rock	3.970	1.436	30	9.3 ± 0.3
Ket-141	Two-pyroxene–hornblende andesite	6221.45	376.50	whole rock	1.249	0.454	59	9.3 ± 0.6
Ket-138	Two-pyroxene andesite	6224.85	376.00	whole rock	1.085	0.391	76	9.2 ± 0.7
Ket-206A	Clinopyroxene–biotite welded tuff	6223.30	367.45	biotite	6.856	2.445	67	9.2 ± 0.5
Ket-204C	Two-pyroxene–hornblende–biotite dacite	6223.15	367.20	whole rock	1.601	0.516	65	8.3 ± 0.5
Ket-146	Hornblende–biotite dacite	6218.95	368.85	whole rock	2.259	0.682	48	7.8 ± 0.4
Ket-126A	Two-pyroxene–hornblende andesite dike	6219.85	379.00	whole rock	0.589	0.149	83	6.5 ± 1.7
E-2585	Clinopyroxene andesite porphyry	6225.40	376.30	whole rock	1.704	0.395	64	6.0 ± 0.4
<u>Late Hornblende Dike unit</u>								
Ket-142B	Andesite dike	6223.90	375.30	whole rock	1.681	0.205	92	3.1 ± 0.8
<u>Intrusive units (see Kurtz et al., 1997, for additional Ar/Ar ages)</u>								
E-2633	Andesite sill	6213.25	377.85	whole rock	0.614	0.266	61	11.1 ± 1.2
Ket-89	Hornblende diorite porphyry	6230.20	377.15	whole rock	1.814	0.748	70	10.6 ± 0.7
Ket-158C	Granodiorite sill	6214.30	372.55	whole rock	2.935	1.127	36	9.8 ± 0.4
Ket-123	Biotite–hornblende granodiorite	6213.10	377.45	whole rock	3.570	1.298	63	9.3 ± 0.4
E-2786	Silicified quartz diorite	6249.40	372.75	whole rock	2.338	0.850	76	9.3 ± 0.7

Notes: All ages determined at SERNAGEOMIN in Santiago, Chile. See Gana et al. (1999) for references to analytical methods. UTM—Universal Transverse Mercator grid points.

(1999) argued that this high rate corresponds to a time of crustal shortening related to inversion of extensional faults in the Coya Machalí Formation and in Mesozoic sequences to the east. Contemporaneous backarc contraction is consistent with foreland-basin deposits as old as ca. 15.7 Ma in the Aconcagua fold-thrust belt (32.5°–34°S, Fig. 1; Irigoyen et al., 2000) and ca. 13.9–13.5 Ma volcanic flows that cover Miocene thrusts in the western Malargue fold-thrust belt (34°S–35°S, Fig. 1; Baldauf, 1997; Baldauf et al., 1997; Pérez, 2000).

#### Middle to Late Miocene: Reestablished Arc Front to the East

The third magmatic group in Table 1 includes the middle to late Miocene volcanic rocks of the arc that began forming at ca. 15 Ma, ~25–30 km east of the early Miocene (Coya Machalí Forma-

tion) arc front (Fig. 2). To avoid nomenclature problems in the use of the term “Farellones Formation,” Godoy (1993) assigned these largely andesitic rocks to the Teniente Volcanic Complex. Subsequently, the Kay and Kurtz 1995 CODELCO report (see acknowledgments) and Kay et al. (1999) used the K/Ar ages reported in Table 2 and the chemical data in Table 3 (and in Appendix DR1 and Tables DR1–DR9)<sup>1</sup> to subdivide the Teniente Volcanic Complex into the ca. 14.4–11.5 Ma Maqui Chico Group, ca. 10.7–9.9 Ma Lower Sewell Group, and ca. 9.3–6.5 Ma Upper Sewell Group. The fine-grained, largely granodioritic plutons in the region, whose biotite <sup>40</sup>Ar/<sup>39</sup>Ar ages cluster near ca.

13–11 Ma and ca. 9–7 Ma, are assigned to the contemporaneous Teniente Plutonic Complex (Kurtz et al., 1997; see Fig. 2).

The emplacement of the Teniente Volcanic Complex and the Teniente Plutonic Complex coincided with three distinctive periods in the regional backarc deformational history: (1) The ca. 14.4–11.5 Ma Maqui Chico Group and the ca. 13–11 Ma plutons coincided with the ca. 15–10.6 Ma eastward advance of the backarc thrust front (Baldauf, 1997; Irigoyen et al., 2000; Giambiagi et al., 2001; Giambiagi and Ramos, 2002). (2) The ca. 10.7–9.9 Ma Lower Sewell Group coincided with a virtual lull in backarc thrusting (Giambiagi et al., 2001) and a ca. 11.7–9 Ma reduced sedimentation rate in the foreland basin to the east (Irigoyen et al., 2000). (3) The ca. 9.3–6.5 Ma Upper Sewell Group and ca. 9–7 Ma plutons coincided with uplift of the Frontal Cordillera

<sup>1</sup>GSA Data Repository item 2005021, analytical methods, is available on the Web at <http://www.geosociety.org/pubs/ft2005.htm>. Requests may also be sent to [editing@geosociety.org](mailto:editing@geosociety.org).

TABLE 3. REPRESENTATIVE ANALYSES OF EL TENIENTE TRANSECT AND FARELLONES AREA VOLCANIC UNITS

Sample	Coya Machalí (Abanico) Formation							Farellones area					
	CM-11	CM-8	CM-5	Fresh CM-7B	Altered CM-7A	CM-4	ETP-10B	TF-4	33°20' to 33°32'S, 70°16' to 70°19'W				
	TF-7	TF-3	TF-10	TF-2	TF-11								
SiO <sub>2</sub>	50.66	56.41	59.30	60.95	59.90	66.96	57.69	50.62	52.32	53.52	55.77	59.90	60.96
TiO <sub>2</sub>	1.24	1.20	0.92	1.16	1.15	0.75	0.82	1.06	1.05	0.98	0.95	1.04	0.90
Al <sub>2</sub> O <sub>3</sub>	18.71	17.57	17.87	16.67	16.80	16.77	18.47	19.42	18.10	18.55	18.09	17.08	16.99
FeO*	9.51	8.06	7.73	8.13	8.19	4.72	6.04	8.32	9.37	8.81	7.72	6.66	6.51
MnO	0.23	0.14	0.19	0.16	0.20	0.06	0.12	0.14	0.25	0.21	0.17	0.14	0.15
MgO	3.70	2.38	2.76	1.93	2.49	1.18	3.32	5.41	4.96	3.14	3.74	2.40	2.29
CaO	10.30	6.61	7.02	4.33	5.23	5.64	8.16	9.61	8.77	7.34	7.20	5.70	5.84
Na <sub>2</sub> O	3.34	4.55	3.81	4.83	4.23	2.87	4.65	3.47	3.73	4.09	3.90	4.46	4.06
K <sub>2</sub> O	0.24	1.59	0.17	1.48	1.54	0.86	0.48	0.93	1.03	1.57	1.38	1.92	2.09
P <sub>2</sub> O <sub>5</sub>	0.29	0.48	0.22	0.35	0.28	0.19	0.26	0.25	0.19	0.26	0.19	0.33	0.22
Volatiles													
Total	98.22	98.99	100.00	100.00	100.00	100.00	100.00	99.23	99.76	98.47	99.11	99.63	100.01
La	12.4	21.0	9.1	13.5	13.8	22.2	5.8	9.2	11.9	13.2	13.4	19.6	15.9
Ce	30.0	49.5	22.5	32.9	33.2	54.4	14.1	22.2	28.1	31.4	30.7	46.9	35.1
Nd	18.5	31.7	13.1	20.4	20.0	28.3	9.1	13.9	16.6	19.5	18.5	26.6	19.4
Sm	4.50	7.29	3.66	5.53	5.39	7.49	2.57	3.37	4.22	4.90	4.23	6.31	4.48
Eu	1.30	2.02	1.19	1.63	1.60	2.07	0.86	1.03	1.13	1.30	1.10	1.59	1.12
Tb	0.741	1.098	0.649	0.919	0.997	1.324	0.413	0.490	0.715	0.853	0.637	0.912	0.708
Yb	2.52	3.88	2.39	3.37	3.61	4.90	1.42	1.48	2.70	2.95	2.37	2.90	2.65
Lu	0.359	0.545	0.316	0.475	0.515	0.687	0.217	0.211	0.375	0.397	0.334	0.420	0.357
Rb													
Sr	417	396	429	388	403	340	647	677	439	387	379	385	312
Ba	146	465	146	535	494	223	218	256	466	524	391	602	477
Pb													
Cs	0.2	0.3	0.1	0.4	0.4	4.0	0.3	0.2	0.7	0.5	1.2	0.9	1.0
U	0.8	1.3	0.4	0.9	0.9	1.4	1.4	0.4	1.0	1.2	1.3	1.9	2.2
Th	2.2	3.8	1.4	2.6	2.6	4.9	5.3	1.5	3.1	3.8	3.9	5.8	6.5
Hf	2.7	4.5	2.4	3.4	3.5	6.3	4.2	2.0	3.2	3.9	3.4	4.8	4.1
Sc	32	23	21	29	28	19	14	28	36	29	22	20	19
Ta	0.42	0.54	0.17	0.28	0.27	0.60	0.36	0.12	0.20	0.27	0.28	0.46	0.37
Cr	43	3	2	1	1	<1	2	54	142	35	15	13	5
Ni	11	7	<1	4	4	<1	8	27	21	10	6	11	4
Co	28	16	17	13	13	6	9	32	33	24	24	15	17
FeO/MgO	2.57	3.39	2.80	4.21	3.29	4.00	1.82	1.54	1.89	2.81	2.06	2.78	2.84
Ba/La	11.8	22.1	16.1	39.5	35.8	10.1	37.7	27.8	39.1	39.8	29.1	30.7	29.9
La/Sm	2.8	2.9	2.5	2.4	2.6	3.0	2.3	2.7	2.8	2.7	3.2	3.1	3.6
Eu/Eu*	0.89	0.88	0.97	0.90	0.88	0.83	1.04	0.98	0.81	0.80	0.82	0.81	0.78
Sm/Yb	1.78	1.88	1.53	1.64	1.49	1.53	1.81	2.27	1.56	1.66	1.78	2.17	1.69
La/Yb	4.9	5.4	3.8	4.0	3.8	4.5	4.1	6.2	4.4	4.5	5.7	6.8	6.0
Ba/Ta	351	860	838	1896	1838	370	608	2216	2304	1953	1420	1314	1307
La/Ta	30	39	52	48	51	37	16	80	59	49	49	43	44
Th/U	2.9	3.0	3.8	3.0	2.8	3.6	3.8	3.6	3.1	3.2	2.9	3.1	3.0
Age (Ma)	20.5 ± 0.8			23.2 ± 0.7									

on thick-skinned thrusts at ca. 9 Ma (Fig. 1; Giambiagi et al., 2001), as well as with out-of-sequence thrusting on the El Fierro fault near the arc (Fig. 2; Godoy et al., 1999) and in the backarc Aconcagua belt (Giambiagi et al., 2001; Giambiagi and Ramos, 2002). The last period was further coincident with a high exhumation rate (~3 mm/yr) in the arc as inferred from  $8.4 \pm 0.3$  Ma biotite and  $7.7 \pm 0.1$  Ma K-feldspar  $^{40}\text{Ar}/^{39}\text{Ar}$  ages in the Nacimiento Rio Cortaderal pluton (Fig. 2; Kurtz et al., 1997), and rapid uplift as inferred from studies of fluid inclusions (Skewes and Holmgren, 1993) and fossil trees (Pons and Vicente, 1985).

#### Late Miocene to Pliocene: Waning and Eastward Migration of Magmatism in a Contractual Regime

The fourth group in Table 1 incorporates the magmatic rocks emplaced in the waning stages of the Teniente Volcanic Complex arc before the SVZ arc front was stabilized ~50 km to the east (Fig. 2). Included in this group are the largely granodioritic plutons of the Young Plutonic Complex whose emplacement ages are constrained by biotite  $^{40}\text{Ar}/^{39}\text{Ar}$  ages of  $6.6 \pm 0.1$  Ma (Jeria pluton) and  $5.5 \pm 0.2$  Ma (Cruz de Piedra pluton) in Kurtz et al. (1997). Associated

with the terminal stages of the Young Plutonic Complex are the magmatic hydrothermal breccias and felsic porphyries related to the El Teniente copper deposit (Cuadra, 1986; Skewes et al., 2002). Maksaeu et al. (2003) used SHRIMP (sensitive high-resolution ion microprobe) U/Pb zircon ages to define crystallization ages of  $6.4 \pm 0.11$ – $6.11 \pm 0.13$  Ma,  $5.28 \pm 0.10$  Ma, and  $4.82 \pm 0.09$  Ma for the felsic intrusions and a combination of SHRIMP U-Pb zircon,  $^{40}\text{Ar}/^{39}\text{Ar}$ , and Re-Os ages to argue that mineralization occurred between 6.3 and 4.4 Ma. The youngest magmatic rocks in the region are postmineralization hornblende-bearing basaltic

Teniente Volcanic Complex (Farellones Formation)

Sample	Maqui Chico Group					Lower Sewell Group					Upper Sewell Group					Late Hornblende dikes			Tentative porphyries	
	Aravena		M. Chico Guanaco			Castillo		Sewell	Sewell	Castillo	Sewell	Sewell	Sewell	Durazno	Sewell	Sewell	ET-2	ET-17		ET-12C
	KET-74	KET-69	KET-52	KET-25	TTE-75	TTE-72	KET-157A	TTE-70	Sewell	Sewell	Castillo	KET-113	KET-110	KET-207	KET-139A	KET-144				
SiO <sub>2</sub>	47.75	51.10	56.47	63.70	70.53	74.52	53.42	53.59	59.90	64.63	53.66	55.39	58.76	59.73	63.38	58.28	67.13	67.24	66.74	
TiO <sub>2</sub>	0.98	1.20	0.93	0.57	0.20	0.19	1.04	1.09	0.83	0.63	1.03	0.93	0.86	0.70	0.56	0.92	0.49	0.42	0.53	
Al <sub>2</sub> O <sub>3</sub>	16.59	20.37	18.37	17.54	13.90	13.85	18.93	17.45	17.96	15.51	18.64	18.27	18.49	19.62	16.29	17.61	17.68	17.09	17.47	
FeO*	7.88	8.37	7.02	4.14	1.32	1.24	7.79	8.64	5.28	5.30	8.10	6.59	5.36	5.03	4.08	5.34	2.83	2.53	2.52	
MnO	0.22	0.19	0.17	0.10	0.06	0.04	0.14	0.14	0.09	0.10	0.19	0.14	0.08	0.06	0.08	0.16	0.12	0.31	0.02	
MgO	2.32	2.87	3.45	1.38	0.36	0.22	3.58	4.36	1.86	1.39	3.33	3.96	2.60	1.61	2.01	3.46	1.39	0.82	1.27	
CaO	9.21	10.79	7.17	3.71	1.57	1.51	8.13	7.51	5.10	4.13	7.01	7.41	6.56	5.19	4.67	7.96	2.65	5.03	4.17	
Na <sub>2</sub> O	3.04	3.13	3.69	4.34	3.61	3.80	4.25	3.42	4.39	3.30	4.40	4.26	4.48	4.36	3.55	3.76	5.32	2.41	5.09	
K <sub>2</sub> O	2.14	0.37	1.01	2.86	3.84	3.54	1.19	1.98	2.17	2.86	1.29	1.40	1.96	2.23	2.68	2.19	2.21	4.02	2.03	
P <sub>2</sub> O <sub>5</sub>	0.20	0.22	0.20	0.19	0.07	0.08	0.21	0.26	0.20	0.16	0.30	0.23	0.08	0.17	0.14	0.31	0.19	0.15	0.16	
volatiles	8.98	0.65	1.16	1.00	4.08	0.77	0.59	0.90	0.93	1.01	0.92	0.75	0.81	2.12						
Total	99.31	99.26	99.64	99.53	99.54	99.76	99.27	99.34	98.71	99.02	98.87	99.33	99.24	99.51	99.56	100.00	100.00	100.00	100.00	
La	10.0	8.8	16.0	21.4	17.2	18.5	13.4	15.4	13.8	18.5	15.1	13.6	18.7	19.5	13.9	17.9	10.0	18.3	14.7	
Ce	22.3	21.0	34.9	37.4	29.7	29.8	27.0	32.0	29.8	36.9	31.9	29.6	40.0	39.4	30.1	41.8	22.3	41.0	31.3	
Nd	14.3	14.1	20.0	19.0	9.5	10.1	15.6	20.1	15.5	18.3	18.2	16.0	25.5	21.2	12.4	22.0	11.4	20.7	15.3	
Sm	3.94	4.17	5.10	4.33	1.80	1.82	4.13	5.05	3.97	4.54	4.39	4.01	4.83	4.61	2.95	4.24	2.10	3.69	2.53	
Eu	1.07	1.27	1.10	0.99	0.41	0.42	1.15	1.08	0.91	0.96	1.20	1.01	1.21	1.04	0.70	1.12	0.59	0.94	0.63	
Tb	0.546	0.559	0.650	0.530	0.189	0.175	0.538	0.671	0.530	0.633	0.551	0.443	0.605	0.508	0.406	0.408	0.158	0.271	0.215	
Yb	1.76	1.81	1.90	2.08	0.85	0.85	1.70	2.22	1.83	2.52	1.65	1.29	1.67	1.48	1.08	0.83	0.29	0.42	0.50	
Lu	0.261	0.245	0.273	0.300	0.130	0.122	0.245	0.316	0.280	0.358	0.220	0.180	0.243	0.219	0.154	0.109	0.038	0.051	0.056	
Rb	104	8	32	104	100	93	26	64	78	75	30	36		68	99					
Sr	270	520	470	360	240	220	540	450	380	270	560	580	621	540	393	762	580	341	798	
Ba	520	280	240	470	530	510	300	320	660	370	390	350	511	490	484	461	597	871	763	
Pb	2	< 1	21	10	12	13	2	3	10	24	8	4		8	10					
Cs	8.4	0.3	1.4	12.9	7.3	5.2	0.7	5.8	3.6	2.0	0.7	0.9	2.6	2.9	8.5	15.6	6.3	6.4	3.8	
Co	0.5	0.5	1.9	2.5	3.9	3.8	0.7	1.8	1.9	2.3	1.1	1.2	2.2	2.2	3.4	0.7	1.4	1.5	1.8	
Th	2.1	1.7	6.3	10.1	13.4	13.0	2.7	6.9	6.3	9.1	3.9	4.0	7.2	7.9	10.7	2.6	3.4	3.5	4.0	
Hf	2.0	2.0	4.0	4.2	8.0	6.9	2.7	5.3	4.5	4.3	3.5	3.0	4.3	4.3	3.6	3.6	2.9	2.8	3.4	
Sc	20	23	18	8	2	2	21	23	15	13	16	17	15	11	10	12	4	4	5	
Ta	0.21	0.23	0.59	0.69	0.47	0.44	0.23	0.33	0.68	0.38	0.22	0.39	0.33	0.37	0.32	0.23	0.18	0.17	0.16	
Cr	19	20	38	12	5	5	22	58	9	23	< 5	85	31	126	19	77	12	11	9	
Ni	9	20	72	25	1	1	22	32	9	23	4	85	22	126	11	49	10	5	7	
Co	25	44	38	21	2	1	24	28	35	26	20	32	18	15	14	19	2	2	6	
FeO/	3.40	2.92	2.03	3.00	3.66	5.63	2.18	1.98	2.84	3.81	2.43	1.66	2.06	3.12	2.03	1.55	2.04	3.08	1.99	
MgO																				
Ba/La	51.8	31.8	15.0	22.0	30.8	27.6	22.4	20.8	47.8	20.0	25.8	25.7	27.3	25.1	34.8	25.8	59.7	47.6	51.9	
La/Sm	2.5	2.1	3.1	4.9	9.6	10.2	3.2	3.0	3.5	4.1	3.4	3.4	3.9	4.2	4.7	4.2	4.8	5.0	5.8	
Eu/Eu*	0.89	1.00	0.72	0.77	0.82	0.85	0.93	0.71	0.76	0.69	0.92	0.88	0.84	0.79	0.77	0.97	1.11	1.03	0.95	
Sm/Yb	2.24	2.30	2.68	2.08	2.12	2.14	2.43	2.27	2.17	1.80	2.66	3.11	2.89	3.11	2.73	5.14	7.34	8.87	5.11	
La/Yb	5.7	4.9	8.4	10.3	20.2	21.8	7.9	6.9	7.5	7.3	9.2	10.5	11.2	13.2	12.9	21.7	35.0	44.0	29.7	
Ba/Ta	2476	1217	407	677	1123	1167	1288	973	971	974	1741	888	1567	1321	1526	1976	3254	5052	4731	
La/Ta	48	38	27	31	36	42	57	47	20	49	67	35	57	53	44	77	54	106	91	
Th/U	4.4	3.2	3.3	4.1	3.4	3.4	3.6	3.8	3.3	4.0	3.6	3.3	3.3	3.6	3.2	3.5	2.4	2.3	2.2	
Age (Ma)				12.3 ± 0.5			10.3 ± 0.8													

*Note:* Analyses for samples with KET and TTE prefixes from U.S. Geological Survey laboratory in Reston, Virginia. Other samples—major elements by electron-microprobe analyses of glasses from rock powders and trace elements by INAA (instrumental neutron activation analysis) in Ward Laboratory at Cornell University. See Kay et al. (1987, 1999) for analytical details. Sample locations in Table DRT-DR9 (see footnote 1 in text). Ages from Charrier et al. (1979) and Table 2.



andesitic to dacitic dikes that are locally referred to as the Late Hornblende Dike unit. K-Ar ages for them are  $3.8 \pm 0.3$  Ma and  $2.9 \pm 0.6$  Ma (Cuadra, 1986) and  $3.1 \pm 0.8$  Ma (Table 2). Maksaeve et al. (2003) reported an  $^{40}\text{Ar}/^{39}\text{Ar}$  age of  $3.85 \pm 0.18$  Ma for the youngest dike in the El Teniente mine.

### Latest Pliocene to Holocene: Reestablished Arc Front to the East

The most recent magmatic rocks in Table 1 fall in two groups. The first consists of the small-volume ca. 2.3–1.8 Ma Bajo Cachapoal pyroxene-bearing basaltic andesite flows that erupted through the western belt of the Coya Machali Formation (Fig. 2) in the forearc of the SVZ (Charrier and Munizaga, 1979). The sec-

ond comprises the Pleistocene to Holocene arc centers of the northern SVZ to the east (Fig. 1).

### CHEMICAL AND ISOTOPIC CHARACTERISTICS OF EL TENIENTE TRANSECT MAGMATIC ROCKS

The most distinctive chemical and isotopic characteristics of the magmatic groups in Table 1 are described below with the goal of singling out the properties that are most indicative of magma sources and pressure- and temperature-sensitive residual mineral assemblages in equilibrium with the magmas. Trends in immobile, low-solubility elements (e.g., Ta, Th, and REEs [rare earth elements]) are emphasized to minimize issues related to hydrothermal alteration. In lieu of modeling

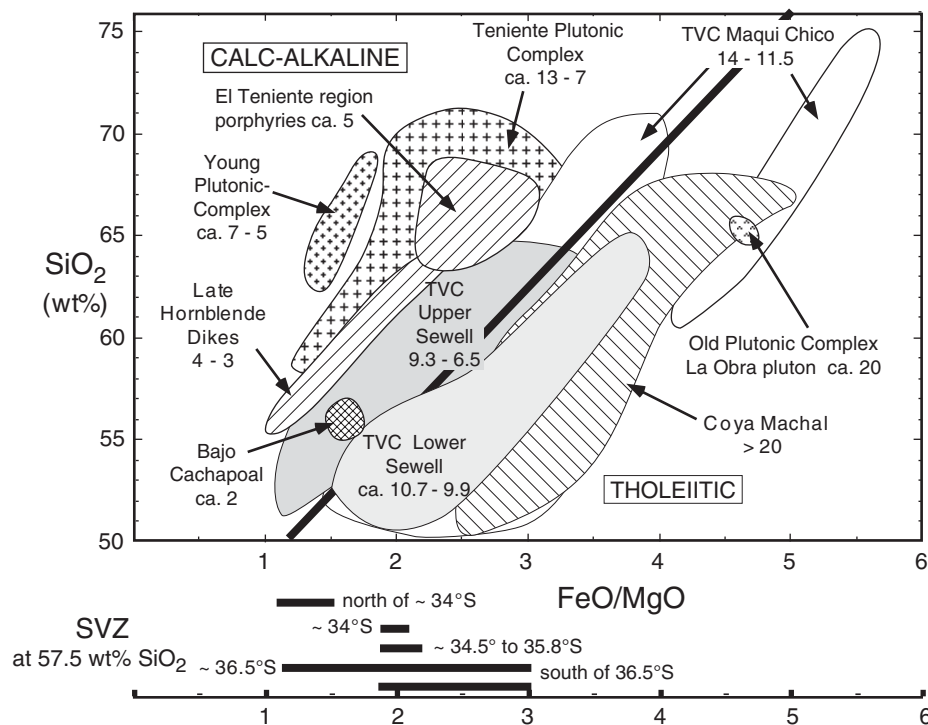
trace element and isotopic trends in partially altered samples, distinctive trends of immobile elements within and between groups are compared to published models for unaltered samples in similar settings elsewhere. Discussions of the modeling and relevant distribution coefficients can be found in the cited papers. Overall, the whole-rock major and trace element analyses in Table 3 and Tables DR1–DR9 (see footnote 1) (~160 analyses including ~60 from Kurtz et al., 1997; Kay et al., 1999; and Stern and Skewes, 1995) and the isotopic data in Table 4 show that the El Teniente region samples display the commonly accepted characteristics of arc magmas (e.g., high Al, alkali, alkaline-earth, U, and Th concentrations; Ti group element [e.g., Ti, Ta, Nb] depletions relative to the REEs [e.g., La/Ta > 25]).

TABLE 4. Sr, Nd, AND Pb ISOTOPE RATIOS OF EL TENIENTE TRANSECT MAGMATIC UNITS

Sample	Location	SiO <sub>2</sub>	Age (Ma)	<sup>143</sup> Nd/ <sup>144</sup> Nd	Error (%)	ε <sub>Nd</sub>	<sup>87</sup> Sr/ <sup>86</sup> Sr	Error (%)	<sup>87</sup> Sr/ <sup>86</sup> Sr <sub>i</sub>	<sup>206</sup> Pb/ <sup>204</sup> Pb	<sup>207</sup> Pb/ <sup>204</sup> Pb	<sup>208</sup> Pb/ <sup>204</sup> Pb
Coya Machali Formation. Camino del Cobre–Rancagua–Colon <sup>†</sup>												
CM-3	km 29.6	48.48	~20	0.512957	0.0010	+6.2	0.703607	0.0008	0.703600			
CM-7A	km 11.7	64.29	23.2	0.512906	0.0011	+5.2	0.703628	0.0007	0.703500			
CME-1B	33°24.7'S 70°14.3'W	55.36	15.9	0.512870	0.0009	+4.5	0.703872	0.0006	0.703770			
Old Plutonic Complex—La Obra pluton. See Kurtz et al. (1997) for age and sample locations												
ETP-1	33°35.8'S 70°29.4'W	73.15	19.6	0.512876	0.0010	+4.6	0.704005	0.0007	0.703610	18.453	15.554	38.210
Farellones Formation near 33°20'S—region of Farellones, Valle Nevado, La Parva												
TF-7	33°20.3'S 70°17.2'W	52.32	~18	0.512889	0.0009	+4.9	0.703815	0.0007	0.703770			
TF-3	33°19.5'S 70°16.6'W	53.52					0.703649	0.0007	0.703560			
TF-10	33°21.6'S 70°15.1'W	55.77	~18	0.512833	0.0009	+3.8	0.703902	0.0007	0.703820			
TF-2	33°31.8'S 70°18.9'W	59.90	~18	0.512907	0.0009	+5.2	0.703734	0.0007	0.703620			
TF-11	33°21.4'S 70°19.0'W	61.61	~18				0.703833	0.0007	0.703690			
Farellones Formation—El Teniente region. See Godoy (1993) for age <sup>†</sup>												
TTE-93	Intrusive	57.11	15.2	0.512919	0.0009	+5.5	0.703980	0.0007	0.703670			
Teniente Volcanic Complex. Ages in Table 3 <sup>†</sup>												
KET-54	Maqui Chico	56.10	13.9	0.512817	0.0009	+3.5	0.704054	0.0007	0.703950			
KET-25	Maqui Chico—C. Guanaco	63.70	12.3	0.512790	0.0009	+3.0	0.704191	0.0007	0.704050			
KET-154	Lower Sewell—C. Castillos	53.36	10.5	0.512824	0.0009	+3.6	0.703995	0.0007	0.703980			
KET-143	Lower Sewell	53.62	~10	0.512800	0.0009	+3.2	0.703913	0.0005	0.703900	18.556	15.579	38.330
KET-141	Upper Sewell	60.21	~9	0.512777	0.0009	+2.7	0.703977	0.0007	0.703930			
KET-146	Upper Sewell—Ag. Frias	63.31	7.8	0.512784	0.0009	+2.8	0.704000	0.0007	0.703920			
KET-126A	dike in Upper Sewell	57.25	6.5	0.512791	0.0009	+3.0	0.703692	0.0007	0.703960	18.565	15.593	38.378
Teniente Plutonic Complex. See Kurtz et al. (1997) for ages and sample locations												
ETP-10A	Alfalfalito	64.10	12.3	0.512765	0.0009	+2.5	0.704293	0.0007	0.704160			
ETP-123	B. Paredones	66.60	9.3	0.512794	0.0009	+3.0	0.704396	0.0008	0.704130			
ETP-9	Carlota	64.04	8.7	0.512782	0.0008	+2.8	0.704022	0.0007	0.703920	18.558	15.582	38.362
ETP-12	Extravio	63.29	8.1	0.512758	0.0007	+2.3	0.703975	0.0006	0.703890	18.558	15.578	38.350
ETP-7	Nac. Rio Cortaderal	67.61	8.4	0.512718	0.0008	+1.6	0.704050	0.0006	0.703980	18.577	15.587	38.388
Young Plutonic Complex. See Kurtz et al. (1997) for ages and sample locations												
ETP-11	Jeria	62.80	6.6	0.512663	0.0009	+0.49	0.704435	0.0007	0.704440	18.588	15.577	38.378
ETP-14	Casa de Piedra	65.80	5.5	0.512634	0.0009	−0.08	0.704273	0.0007	0.704240			
ETP-15	Cerro Cathedral	69.24	~5	0.512676	0.0010	+0.74	0.704409	0.0007	0.704370			
Late Hornblende dikes. See Table 3 <sup>†</sup>												
KET-142B	El Teniente Mine	55.81	3.1	0.512647	0.0010	+0.18	0.704350	0.0007	0.704350			
ET-2	El Teniente Mine	55.45	3.5	0.512689	0.0010	+1.0	0.704175	0.0007	0.704160	18.597	15.590	38.410
ET-5	El Teniente Mine	65.20	3.5	0.512682	0.0009	+0.86	0.704098	0.0007	0.704090	18.608	15.613	38.508

Note: Ages are estimates when indicated by ~. ε<sub>Nd</sub> based on CHUR (chondritic uniform reservoir) value of 0.512628 and ε<sub>Nd</sub> value of −15.15 for La Jolla. See Appendix DR1 (see footnote 1 in text) and Kurtz et al. (1997) for further analytical details.

<sup>†</sup>Sample locations are available in Tables DR1–DR9 (see footnote 1 in text).



**Figure 3.** Plot of FeO/MgO ratio vs. weight percent SiO<sub>2</sub> for El Teniente transect volcanic and plutonic rocks of Teniente Volcanic Complex (TVC) relative to Miyashiro's (1974) calc-alkaline and tholeiitic fields (separated by diagonal black line). The range of FeO/MgO ratios in Quaternary to Holocene SVZ magmas with ~57.5% SiO<sub>2</sub> at the given latitudes is shown below the plot. Note the overall progression from the tholeiitic to the calc-alkaline field in early Miocene to Pliocene El Teniente transect magmatic units (ages in Ma in labels) and from south to north in SVZ centers. Data for El Teniente transect are from Table 3 and Tables DR1–DR9 (see footnote 1 in the text), Kurtz et al. (1997), and Stern and Skewes (1995). Data for SVZ centers are from compilations in Hildreth and Moorbath (1988) and Dungan et al. (2001).

As many of the samples are partially altered, a key issue is the extent to which hydrothermal alteration has been a factor in their final chemistry. It is important to note that, as is common in alteration processes involving hydrothermal circulation of low-salinity, meteoric water, only very mobile elements like Cs and Rb appear to be very affected (e.g., Price et al., 1991). Support for this statement comes from the general chemical coherence of samples within age groups (Figs. 3–5), as well as nearly identical analyses for the fresh interior of a spheroidally weathered basaltic block (locality dated at  $23.2 \pm 0.7$  Ma by Charrier and Munizaga, 1979) of the Coya Machalí Formation and a highly altered adjacent flow (CM7a and CM7b in Table 3). In a more extreme case, a chemical comparison of fresh (KET69; 0.65% volatiles) and altered (KET74; ~9% volatiles) Teniente Volcanic Complex samples shows variations in Ce-normalized trace element concentrations of <10% for REEs (except Eu), Th, Hf, Nb, and U, ~75% for Ba, and >1000% for Rb and Cs.

Samples with few or no original minerals left and that clearly show nonmagmatic chemical trends have been excluded from the discussion and the figures.

The question of trace element mobility is particularly critical for the late Miocene porphyries as their wide range of K<sub>2</sub>O (~3%–7.5%) and Na<sub>2</sub>O (~0.5%–5%) concentrations are typical of hydrothermally altered samples. Support for the concept that the concentrations of their more immobile elements reflect magmatic processes comes from their regular REE patterns that lack the large Ce anomalies typically associated with REE mobility (e.g., Price et al., 1991). Similar light, but distinct heavy, REE patterns also support a magmatic character for the REEs as the more soluble light REEs should be more affected by alteration than the heavy REEs. Other evidence for retention of magmatic features comes from the fact that REE patterns are similar in highly altered breccia clasts and unaltered flows from the Teniente Volcanic Complex. Also, similar chemical

trends exist in altered porphyry and unaltered Young Plutonic Complex samples, and ratios among Ba, Sr, U, and Th are relatively constant in the least altered samples.

### Latest Oligocene to Early Miocene

Distinctive features of the Coya Machalí Formation samples include amphibole-free to amphibole-poor (<2%–3%) phenocryst assemblages; a wide compositional range (47%–67% SiO<sub>2</sub>); FeO/MgO ratios that plot in the arc tholeiitic field of Miyashiro et al. (1974) (Fig. 3); K, Ba, U, and Th concentrations that are typical of low- to medium-K arc magmas (Fig. 4A); and La/Ta (30–60) and Ba/La (20–40) ratios that overlap those of Holocene magmas of the southern SVZ (Hickey et al., 1986). Other distinctive trace element features include nearly parallel REE patterns with flat heavy (Sm/Yb = ~1–2) and moderately positive light (La/Sm = ~1–3) REE slopes, and Eu anomalies that become increasingly negative as La/Sr ratios and SiO<sub>2</sub> contents increase (Fig. 4A). In comparison, La Obra leucogranodiorite samples of the Old Plutonic Complex have similar REE patterns (La/Sm = ~3; Sm/Yb = ~1.5), Eu anomalies (Eu/Eu\* = 0.51) (Figs. 4B and 5), and La/Ta ratios (30–38), but lower FeO/MgO ratios and higher K and Ba contents (López-Escobar et al., 1979; Kurtz et al., 1997). These differences mimic those observed in closely related volcanic and fine-grained plutonic rocks in the Aleutian arc (e.g., Kay et al., 1990). Isotopic ratios listed in Table 4 and plotted in Figures 6–8 for the Coya Machalí Formation and La Obra samples show that they have the highest  $\epsilon_{\text{Nd}}$  values (+6.2 to +4.5) and the lowest  $^{87}\text{Sr}/^{86}\text{Sr}$  (0.7035–0.7037) and  $^{206}\text{Pb}/^{204}\text{Pb}$  (18.45) ratios in the El Teniente transect. Their characteristics generally overlap those of Abanico Formation volcanic rocks from both north and south of the El Teniente transect (Vergara et al., 1999).

In analogy with arc magmas modeled elsewhere (e.g., SVZ, south of ~37°S—Gerlach et al., 1988; Hildreth and Moorbath, 1988; intra-oceanic Aleutian arc—Kay and Kay, 1994), the Coya Machalí Formation and La Obra samples have the chemical features of magmas that formed by relatively high percentages of melting in the mantle wedge and subsequently crystallized and equilibrated with low-pressure mineral assemblages dominated by plagioclase, olivine, and pyroxene in the crust. A role for plagioclase is indicated by negative Eu anomalies that increase with increasing SiO<sub>2</sub> and decreasing Sr contents, and roles for olivine and pyroxene without significant amphibole are shown by nearly parallel REE patterns that increase in level with SiO<sub>2</sub> concentration.

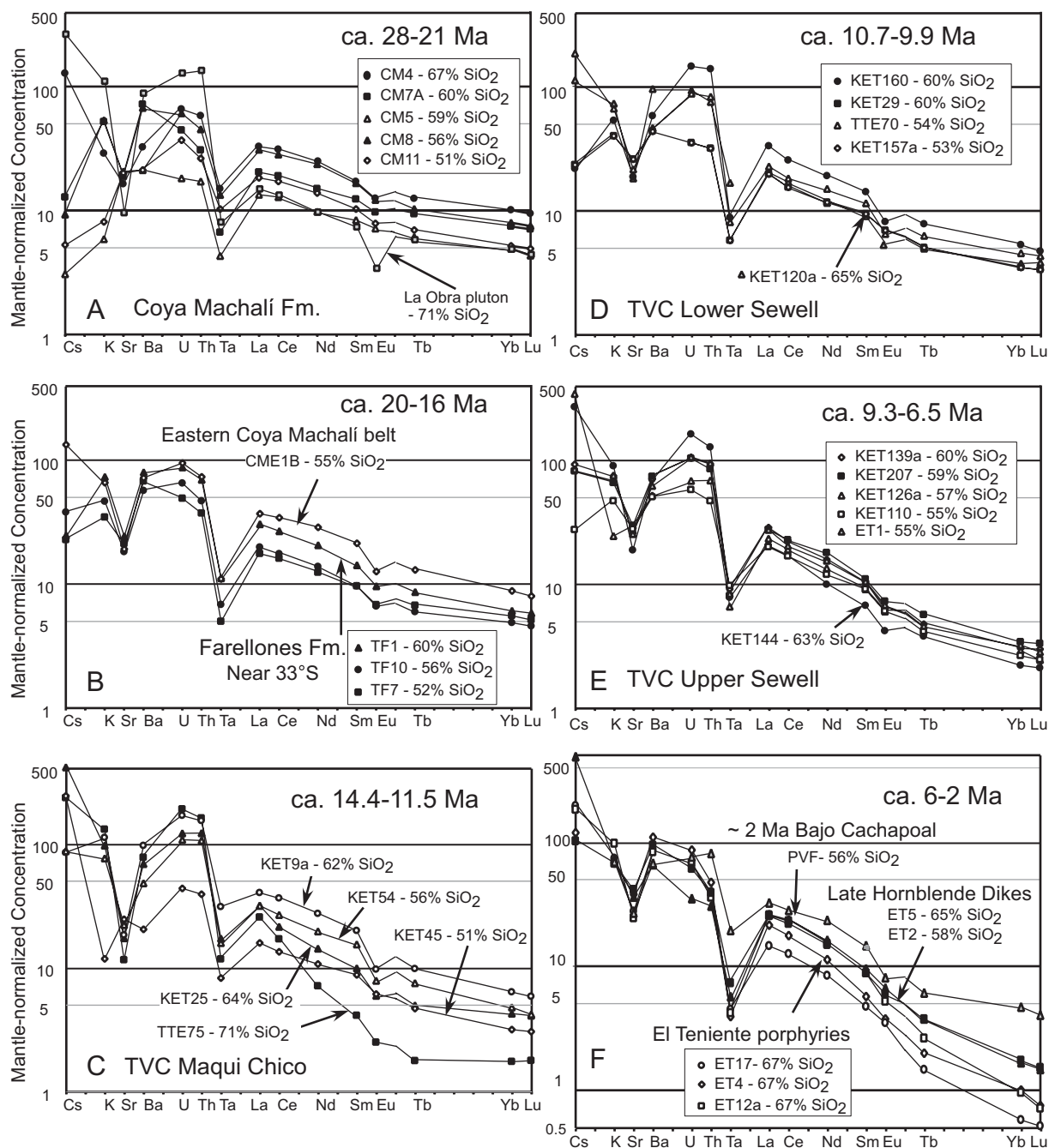


**Figure 4.** Extended trace element diagrams for El Teniente transect samples normalized to mantle values of Sun and McDonough (1989). Values (in ppm) used in normalizations: Cs—0.032; K—250; Ba—3.77; Sr—21.1; U—0.021; Th—0.085; Ta—0.041; La—0.687; Ce—1.775; Nd—1.354; Sm—0.444; Eu—0.168; Tb—0.108; Yb—0.493; Lu—0.074. Note the Ta depletions and Th enrichments typical of arc magmas and the temporal trend from flatter to steeper REE patterns. Bajo Cachapoal data (PVF in part F) from Stern and Skewes (1995); El Teniente transect data from sources listed in Figure 3. See discussion in text. TVC—Teniente Volcanic Complex.

### Middle Miocene to Late Miocene

Middle to late Miocene samples from the Farellones Formation near 33°20'–33°32'S, 70°16'–70°19'W (Fig. 1) and the Teniente Volcanic Complex can be distinguished from early Miocene Coya Machalí Formation samples by

their amphibole-bearing phenocryst assemblages, a temporal trend toward a narrower SiO<sub>2</sub> range, lower FeO/MgO ratios at a given SiO<sub>2</sub> content (Fig. 3), Th and K concentrations like those in medium- to high-K arc magmas, and steeper REE patterns (La/Yb = 5–23; Figs. 4B–4E, 5). The major and trace element

character as well as initial Sr, Nd, and Pb isotope ratios (Table 4; Figs. 6–8) of the oldest samples are most like Coya Machalí Formation samples, whereas the youngest ones are most like Pliocene samples (see below). In accord with this trend,  $\epsilon_{\text{Nd}}$  values in Maqui Chico Group and Lower Sewell Group samples are

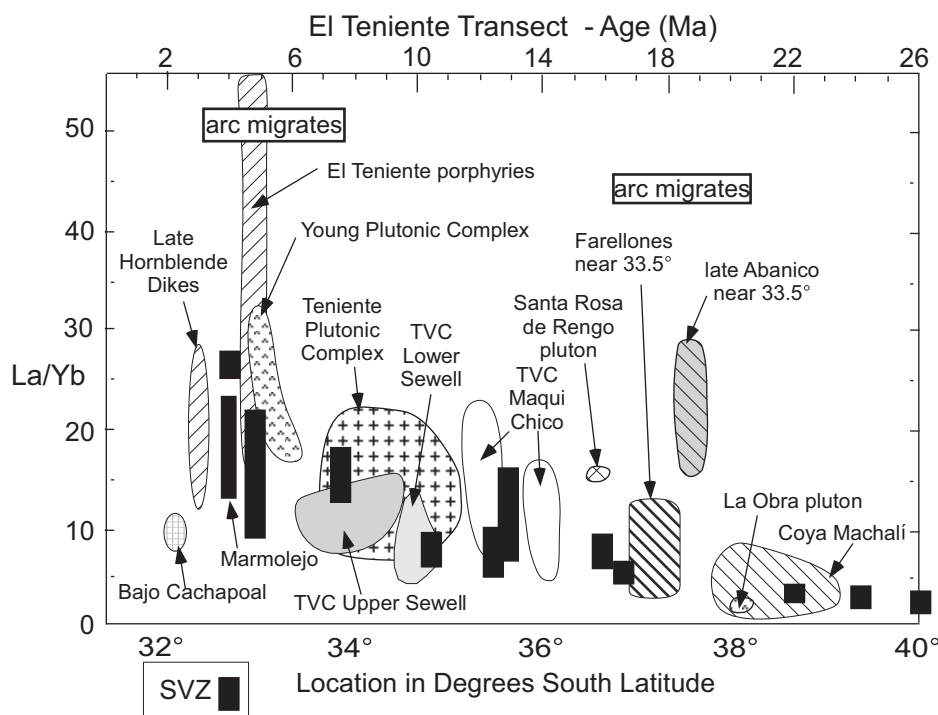


**Figure 5.** Plot of range of La/Yb ratios (measure of steepness of REE pattern) in El Teniente transect magmatic samples (patterned fields) vs. age shown at top and in SVZ volcanic centers (heavy black bars) vs. latitude shown at base. Graph shows that minimum and maximum La/Yb ratios increase with decreasing age in El Teniente transect samples and from south to north along the SVZ. A comparison with Figure 4 shows that variations in La/Yb ratios result from differences in both light and heavy REE slopes. Sources of El Teniente transect data are as in Figure 3; SVZ data are from compilation in Tormey et al. (1991) and references therein; some Marmolejo region data from Ramos et al. (1996a). TVC—Teniente Volcanic Complex.

somewhat higher than those in Upper Sewell Group samples. Among Teniente Volcanic Complex and Teniente Plutonic Complex samples,  $\epsilon_{\text{Nd}}$  values are +3.6 to +2.3,  $^{87}\text{Sr}/^{86}\text{Sr}$  ratios are 0.7039–0.7041, and  $^{206}\text{Pb}/^{204}\text{Pb}$  ratios are 18.55–18.57.

In detail, ca. 19–16 Ma Farellones Formation samples and ca. 14.4–11.5 Ma Maqui Chico Group (Teniente Volcanic Complex) samples are characterized by broad ranges of  $\text{SiO}_2$  contents (50%–74%), FeO/MgO ratios, and trace element characteristics (Figs. 3–5). Among their distinctive trace element features are relatively flat REE patterns at <62%  $\text{SiO}_2$  ( $\text{La}/\text{Sm} = 1.2\text{--}3.7$ ;  $\text{Sm}/\text{Yb} = 1.5\text{--}2.4$ ) that become increasingly light REE enriched ( $\text{La}/\text{Sm}$  to 10) and middle REE depleted as contents of Sr decrease and contents of  $\text{SiO}_2$  increase (Figs. 4B and 4C). Comparisons with trace element models for Mexican arc magmas at El Chichon (Lühr et al., 1984) show that these features are like those in oxidized magmas where residual titanite and apatite have preferentially removed middle REEs and plagioclase has removed Sr, but little Eu, as it is mostly  $\text{Eu}^{+3}$ . Similar characteristics

in Miocene Pocho volcanic rocks in the backarc of the Chilean flat-slab region have been modeled by fractionation of pyroxene, amphibole, plagioclase, and accessory titanite and apatite (Kay and Gordillo, 1994).

Samples of the younger Lower Sewell Group and Upper Sewell Group of the Teniente Volcanic Complex are distinguished from the older samples by their increasingly more amphibole-rich phenocryst assemblages, narrowing  $\text{SiO}_2$  (most 53%–64%) ranges, and decreasing FeO/MgO ratios that result in crossing of the Upper Sewell samples into the calc-alkaline field of Miyashiro (1974) (Fig. 3). Other distinctive features include steeper REE patterns (higher La/Yb ratios; Figs. 4D, 4E, and 5) that reflect both higher La/Sm (Lower and Upper Sewell:  $\sim 2.9\text{--}4.1$  and  $\sim 3.3\text{--}5.1$ , respectively) and Sm/Yb (Lower and Upper Sewell:  $\sim 1.8\text{--}2.7$  and  $\sim 2.6\text{--}3.2$ , respectively) ratios. The contemporaneous Teniente Plutonic Complex granodiorites (59%–70%  $\text{SiO}_2$ ) have similar low FeO/MgO ratios at a given  $\text{SiO}_2$  content (Fig. 3), high K and Th concentrations, and steep light concave REE patterns characterized by high La/Sm

ratios (3.3–6.5). Those granodiorites with K–Ar biotite ages of ca. 13–11 Ma are most like Lower Sewell samples, whereas those with biotite ages of ca. 9–7 Ma are most like Upper Sewell samples. Chemical differences with the volcanic samples again parallel those in arcs elsewhere (e.g., Aleutians; Kay et al., 1990). As shown by many models of similar samples (e.g., Kay et al., 1987, 1991; Hildreth and Moorbath, 1988), the chemical features of the Lower Sewell and Upper Sewell samples are those that are expected when residual amphibole is in the magmatic source or the fractionating mineral assemblage.

### Latest Miocene to Pliocene

Distinctive features among the Young Plutonic Complex (59%–70%  $\text{SiO}_2$ ), the El Teniente porphyries (64%–69%  $\text{SiO}_2$ ), and the Late Hornblende Dike unit (56%–65%  $\text{SiO}_2$ ) are FeO/MgO ratios that plot in the calc-alkaline field (Fig. 3), steep to very steep REE patterns ( $\text{La}/\text{Yb} = \sim 15\text{--}55$ , Fig. 5) that reflect both light REE enrichment and heavy REE depletion (Table 3), small Eu anomalies, high La/Ta ratios, and low Th concentrations (Fig. 4F). The highest La/Ta ratios (to 106) and the steepest REE patterns ( $\text{La}/\text{Yb}$  to 55) with the smallest Eu anomalies (<10%) occur in the dacitic porphyries. Other notable features in this group include high Cr ( $\sim 200$  ppm) and Ni ( $\sim 80$  ppm) concentrations in Late Hornblende Dike unit mafic andesite (55%  $\text{SiO}_2$ ) samples and relatively low  $\epsilon_{\text{Nd}}$  values (+1.0 to –0.1) and high  $^{87}\text{Sr}/^{86}\text{Sr}$  (0.70415–0.70444) and  $^{206}\text{Pb}/^{204}\text{Pb}$  ( $\sim 18.60$ ) ratios in the Young Plutonic Complex and Late Hornblende Dike unit samples (Table 4, Figs. 6–8).

Magmas with chemical features like those in the porphyries and Young Volcanic Complex are now commonly called adakites (Defant and Drummond, 1990). Numerous modeling studies in the Andes (e.g., López-Escobar et al., 1979; Kay et al., 1987, 1991; Hildreth and Moorbath, 1988) and elsewhere (e.g., Aleutians; Kay, 1978; southern California; Gromet and Silver, 1987) have shown that steep REE patterns that are coupled with little to no Eu anomaly and high Sr and Na concentrations can be explained by the last equilibration of these magmas with high-pressure plagioclase-poor, garnet-bearing residual mineral assemblages (see Rapp and Watson, 1995).

The latest Pliocene Bajo Cachapoal forearc basaltic andesites ( $\sim 56\%$   $\text{SiO}_2$ ) analyzed by Stern and Skewes (1995) are distinctive in having somewhat steeper REE patterns ( $\text{La}/\text{Yb} = \sim 10$ ;  $\text{Sm}/\text{Yb} = \sim 2.8$ ) than the early Miocene Coya Machali Formation lavas that they overlie. The Bajo Cachapoal lavas are like the Late Hornblende Dike unit samples in having high



Cr (~100 ppm) and Ni (~50 ppm) contents, but differ in having lower Na contents, flatter REE patterns, and lower La/Ta (28–33) and Ba/La (18–21) ratios (see Figs. 4F and 5). Their most distinctive characteristics are their low  $\epsilon_{\text{Nd}}$  values (–1) and high  $^{87}\text{Sr}/^{86}\text{Sr}$  ratios (0.70485) that overlaps those of Holocene centers in the northern SVZ to the east (Figs. 6 and 8).

## DISCUSSION: ANDEAN MAGMA SOURCES AND TECTONIC PROCESSES

In the discussion below, the regional setting and mineralogical, chemical, and isotopic characteristics of El Teniente transect magmas are compared to, and evaluated relative to, similar south to north trends in SVZ centers. The chemical parallels seen, along with inferences from lithospheric-scale cross sections across the SVZ and regional geologic observations, are used to argue that early Miocene to Holocene trends in El Teniente transect magmas and south to north trends along the SVZ have similar origins. The case is made that both in situ crustal contamination and forearc subduction erosion are needed to explain these trends.

### Chemical and Isotopic Trends in El Teniente Transect and Southern Volcanic Zone Magmatic Rocks

#### Major, Trace Element, and Mineralogical Trends

The temporal trends in El Teniente transect magmas discussed above are highlighted by a progression from low-K tholeiitic to high-K calc-alkaline major element signatures, narrowing major and trace element compositional ranges, a change from pyroxene- to amphibole-dominated mafic phenocryst assemblages in andesitic lavas, and steepening REE patterns. On the basis of published data for SVZ magmas (e.g., López-Escobar et al., 1977; Hickey et al., 1986; Futa and Stern, 1988; Hildreth and Moorbath, 1988; Tormey et al., 1991; Dungan et al., 2001; and references therein), these trends generally parallel those from south to north along the SVZ (Figs. 1, 3, and 5) as shown by the following observations: (1) early Miocene Coya Machali samples are like samples from the southern SVZ south of 37°S; (2) Teniente Volcanic Complex samples are like transitional SVZ samples with middle Miocene Maqui Chico Group samples being most like those from near 36°S, and late Miocene Lower Sewell and Upper Sewell Group samples being most like those from 35°S to 34.5°S; (3) latest Miocene to Pliocene Late Hornblende Dike unit samples are most like SVZ samples near 34°S;

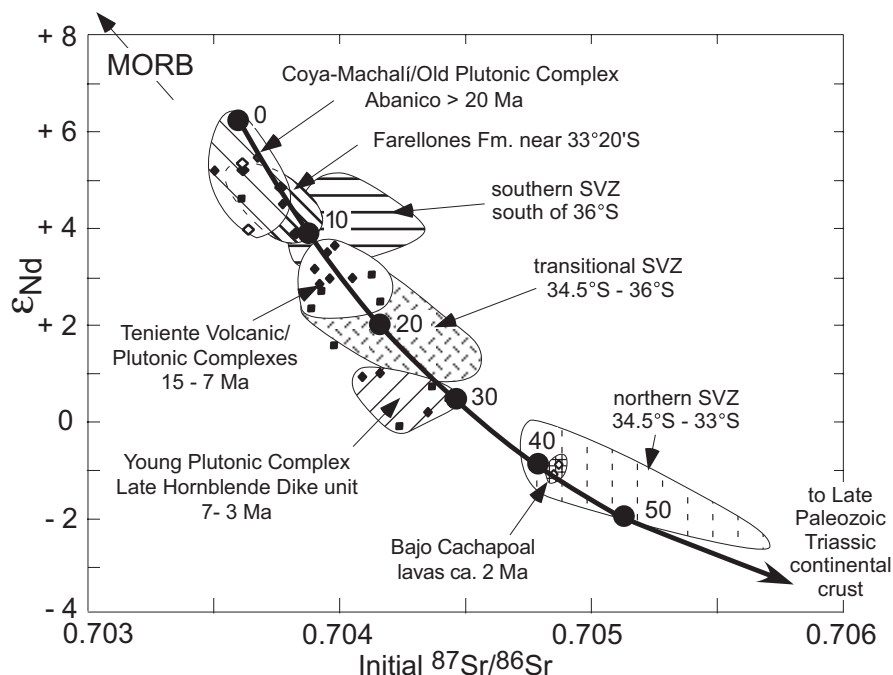


**Figure 6.** Plot of initial  $\epsilon_{\text{Nd}}$  vs. initial  $^{87}\text{Sr}/^{86}\text{Sr}$  for El Teniente transect magmatic rocks, SVZ arc centers, and Paleozoic batholithic samples. Note general trends from low to high  $^{87}\text{Sr}/^{86}\text{Sr}$  and high to low  $\epsilon_{\text{Nd}}$  with decreasing age in the El Teniente transect and from south to north along the SVZ. Curve shows results of a simple mixing model between a basaltic Coya Machali Formation magma and bulk Late Paleozoic-Triassic continental crust. Labeled circles mark percentages of crustal contaminant. Coya Machali Formation end member: Nd and Sr ratios from CM3 in Table 4; 450 ppm Sr and 9 ppm Nd as in typical SVZ basalt (Hickey et al., 1986). Choiyoi contaminant: ca. 220 Ma Choiyoi plutonic rocks with initial ratios of  $^{87}\text{Sr}/^{86}\text{Sr} \sim 0.7058$  and  $\epsilon_{\text{Nd}} \sim -3.5$  (Mpodozis and Kay, 1992; Parada et al., 1999) corrected to 20 Ma by using 58 ppm Rb, 325 ppm Sr, 3.9 ppm Sm, and 20 ppm Nd based on bulk-crustal values in Rudnick and Fountain (1995). El Teniente transect data (filled symbols: diamonds—volcanic rocks; squares—plutons) are from Table 4; Bajo Cachapoal (open diamonds) from Stern and Skewes (1995); and Abanico Formation data (open diamonds) from López-Escobar and Vergara (1997). SVZ fields are based on Hickey et al. (1986), Hildreth and Moorbath (1988), Tormey et al. (1991), Dungan et al. (2001), and references therein. MORB—mid-oceanic-ridge basalt.

(4) El Teniente porphyry samples are unlike any SVZ center; and (5) samples from the forearc Bajo Cachapoal flows and the northernmost SVZ (Tupungato to Maipo centers in Fig. 1) are chemically distinct from each other as well as the rest of the samples.

These broad regional comparisons of SVZ and early Miocene to Pliocene El Teniente transect magmas are intended to emphasize their dominant characteristics in the long tradition of studies along the zone (e.g., Hildreth and Moorbath, 1988, and references above). On a finer scale, the compositions of the magmas from some SVZ centers have been shown to be quite diverse, as documented by exceptionally detailed studies of the Tatara-San Pedro complex near 36°S (e.g., Dungan et al., 2001). A still-outstanding issue is whether this level of

diversity is typical of all the centers, or whether this diversity reflects the complex setting of the Tatara-San Pedro center at the southern end of the transitional SVZ segment (the Tatara-Maipo segment of Dungan et al., 2001; Fig. 1). It is noteworthy that the comparison above pairs the Tatara-San Pedro complex with the chemically diverse Miocene Teniente Volcanic Complex Maqui Chico Group in the El Teniente transect.

The chemical variations in El Teniente transect magmas, like those along the SVZ, can be attributed to first-order changes in the chemistry of the magma source and the residual mineral assemblage that equilibrated with the magmas. One of these changes, which is reflected in the REEs, is a shift in the combined source and fractionating residual mineral assemblage from a low-pressure anhydrous pyroxene-feldspar-dominated



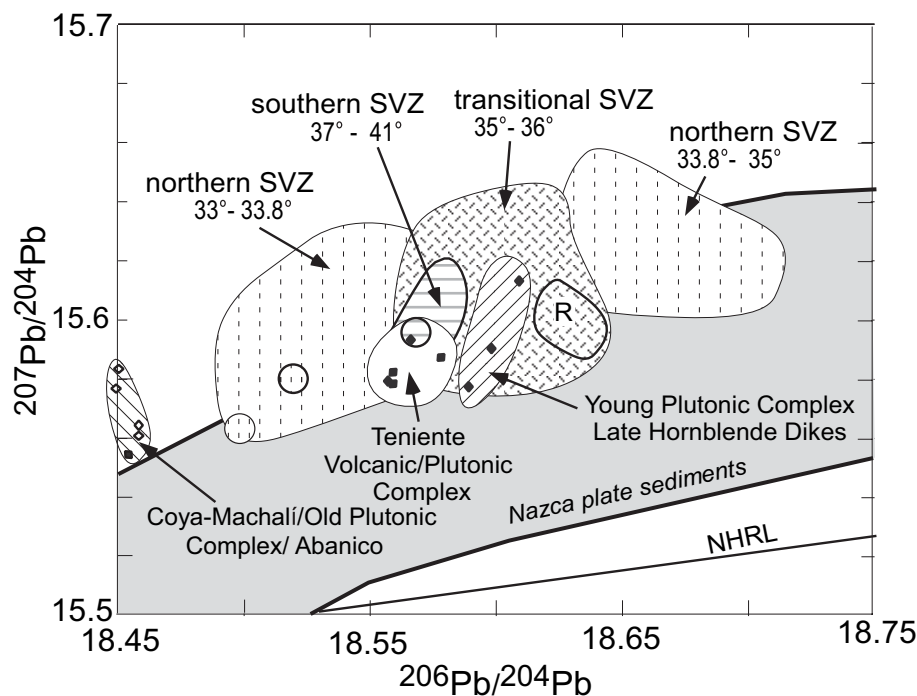


**Figure 7.** Plot of  $^{206}\text{Pb}/^{204}\text{Pb}$  vs.  $^{207}\text{Pb}/^{204}\text{Pb}$  ratios for El Teniente transect samples (data sources and symbols as in Fig. 6) compared to fields for SVZ centers and data from xenoliths and country rocks (large circles), and rhyolites (field labeled R) in corresponding regions (same patterns). These data as well as the field for Nazca plate sediments (light gray field) are from Hildreth and Moorbath (1988). See discussion in text. NHRL—Northern Hemisphere reference line.

assemblage to a medium-pressure hydrous amphibole-feldspar-dominated assemblage to a higher-pressure garnet-bearing, feldspar-poor assemblage. Hildreth and Moorbath (1988) explained this south to north trend along the SVZ with their melting, assimilation, storage, and homogenization (MASH) model that called upon magma equilibration at the base of a progressively thicker crust to the north. Kay et al. (1987, 1991) attributed similar trends in early Miocene to Pliocene magmatic rocks near 30°S over the Chilean flat-slab to magma evolution at the base of a thickening crust over a shallowing subduction zone. Other models for SVZ magmas have emphasized a complementary role for decreasing percentages of partial melt of a cooler, more garnet-rich mantle over a shallower subduction zone to the north (e.g., López-Escobar et al., 1977; Tormey et al., 1991) and mixing of different proportions of subducted sediments or continental crust removed by forearc subduction erosion into the mantle wedge (Stern, 1989, 1991).

#### Isotopic Trends

Changes in  $^{87}\text{Sr}/^{86}\text{Sr}$  ratios and  $\epsilon_{\text{Nd}}$  values in El Teniente transect samples (Table 4; Stern and Skewes, 1995; López-Escobar and Vergara, 1997) also show an early Miocene

to Holocene progression paralleling south to north trends along the SVZ (Fig. 6; data summaries from Hickey et al., 1986; Futa and Stern, 1988; Hildreth and Moorbath, 1988; Stern, 1989; Tormey et al., 1991; Dungan et al., 2001; references therein). Specifically,  $\epsilon_{\text{Nd}}$  values and  $^{87}\text{Sr}/^{86}\text{Sr}$  ratios in (1) early Miocene Coya Machali-La Obra samples either overlap or are more depleted (i.e., higher  $\epsilon_{\text{Nd}}$  and lower  $^{87}\text{Sr}/^{86}\text{Sr}$ ) than those from the SVZ south of 37°S; (2) middle to late Miocene Teniente Volcanic Complex samples overlap those in SVZ centers between 36°S and 34.5°S with Maqui Chico Group samples being most like those from the southern SVZ; (3) latest Miocene to Pliocene Young Plutonic Complex and Late Hornblende Dike unit samples overlap those from SVZ centers near 34°S; and (4) Pliocene Bajo Cachapoal lavas (Stern and Skewes, 1995) overlap those from SVZ centers north of 34°S. As with changes along the SVZ, distinct shifts to lower  $\epsilon_{\text{Nd}}$  values and higher  $^{87}\text{Sr}/^{86}\text{Sr}$  ratios between Coya Machali Formation and Teniente Volcanic Complex samples at ca. 19–16 Ma, and between Teniente Volcanic Complex and late Pliocene–Holocene samples after ca. 7 Ma (Figs. 6 and 8) are nearly independent of  $\text{SiO}_2$ , Sr, and Nd contents (Fig. 8). These shifts thus

reflect differences in compositions and/or amounts of crustal components in the mantle source where the magmas originated. To maintain the narrow range in isotopic values seen across the broad range of  $\text{SiO}_2$  contents in each period (Fig. 8), the evolution of the mafic magmas can involve only minor subsequent crustal contamination or, less likely, only contaminants with low Sr and Nd contents and/or with isotopic ratios like those of the mafic magmas.

In contrast to Nd and Sr isotope ratios, the trend of increasing  $^{206}\text{Pb}/^{204}\text{Pb}$  ratios with decreasing age in El Teniente transect samples has no parallel in south to north changes along the SVZ (Fig. 7). Specifically, the early Miocene Coya Machali Formation samples, which are like SVZ samples south of 36°S in other ways, have the lowest ratios, whereas late Miocene–Pliocene samples that are most like northernmost SVZ centers in most aspects, have ratios like the SVZ centers south of 35°S. Hildreth and Moorbath (1988) argued that Pb isotope ratios in SVZ centers strongly reflect contaminants from the underlying crust, as ratios in mafic samples are like those in basement samples, crustal xenoliths, or coexisting rhyolites at or near a particular center (Fig. 7). A local crustal contaminant is consistent with mass-balance considerations, as Pb is strongly concentrated in feldspar-rich crust compared to peridotite mantle. As the same argument is true for crustal contaminants in the mantle wedge, a subcrustal Pb contribution is difficult to exclude as an additional factor.

End-member models to explain Nd and Sr isotope variations along the SVZ parallel those for major and trace elements. At one extreme is the MASH model that calls upon isotopic homogenization of mantle and crustal components at the base of the thicker, more radiogenic crust in the north (Hildreth and Moorbath, 1988). At the other end are models involving mantle-source mixing that call for contamination of the mantle wedge by subducted sediment or crust removed by forearc subduction erosion (e.g., Stern, 1991). To counter arguments against source-mixing models based on a lack of evidence for different amounts or compositions of subducted sediment along the SVZ (e.g., Hildreth and Moorbath, 1988), Stern (1991) argued for adding similar amounts of crustal contaminants to a thinner mantle wedge above a shallower slab in the north.

Important crustal contaminants in El Teniente transect magmas likely come from the bulk crustal columns related to the granites and rhyolites that crop out in the coastal ranges to the west (late Paleozoic to Early Jurassic granites), in the Frontal Cordillera to the east (late Paleozoic to Triassic Choiyoi Group), and that

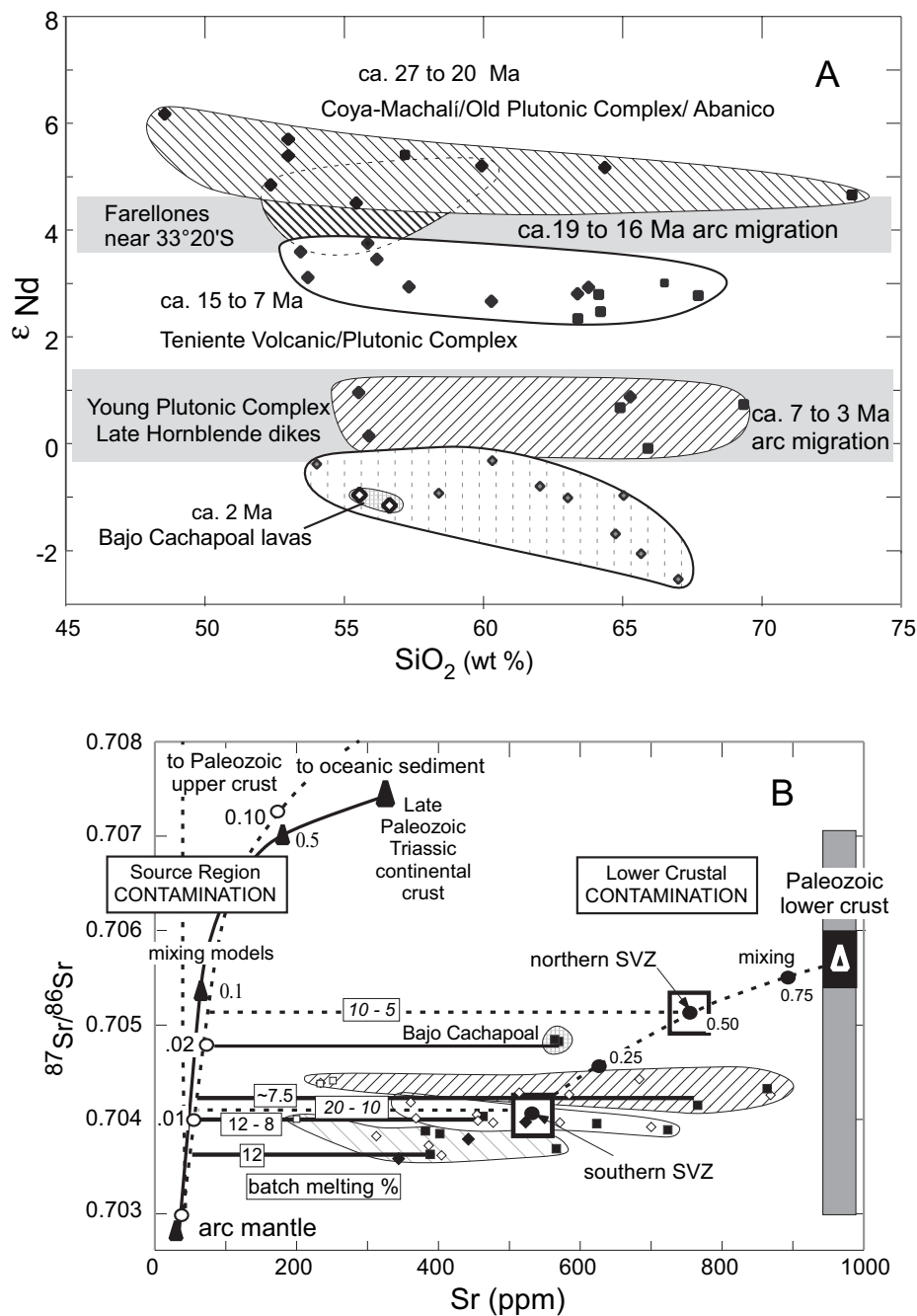


Figure 8. (A) Plot of initial  $\epsilon_{Nd}$  vs. weight percent  $SiO_2$  for El Teniente transect samples (data sources and symbols as in Fig. 6) showing relative constancy of  $\epsilon_{Nd}$  with increasing  $SiO_2$  within magmatic groups. Gray rectangular regions coincide with times of early and late Miocene frontal-arc migration. (B) Plot of initial  $^{87}Sr/^{86}Sr$  vs. Sr (ppm) showing relative constancy of  $^{87}Sr/^{86}Sr$  ratios with variable Sr and  $SiO_2$  contents (diamonds— $SiO_2$  <53%; squares—53%–59%; open diamonds—60%–66%; open squares—60%–66%) within major El Teniente transect age groups (fields as in Fig. 8A). Data are superimposed on plot with models (dashed curves) from Stern (1991) for source region (oceanic sediment and Paleozoic upper crust) and Paleozoic lower-crustal contaminants in SVZ magmas. Stern argued that combined higher Sr contents and  $^{87}Sr/^{86}Sr$  ratios in magmas of the northern compared to the southern segment of the SVZ (two bold boxes) can be explained by lower percentages of batch melting of a mantle-wedge peridotite contaminated by a higher proportion of subducted sediment and/or Paleozoic upper crust (boxed numbers on dashed horizontal lines show melting percentages; lines intersect mixing curves at mixing ratio). The solid curve shows a source-mixing model for arc mantle and Late Paleozoic–Triassic bulk continental crust (composition same as in model in Fig. 6). Solid horizontal lines connect lines with average mafic samples in El Teniente transect fields. Boxed numbers on lines indicate batch-melting percentages. Bajo Cachapoal magmas are better modeled with lower percentages of a more radiogenic source component.

could underlie the entire region (Fig. 1). The general viability of such a contaminant is shown by the simple Sr and Nd isotope mixing model between bulk Choiyoi crust and Coya Machali Formation primitive basalt in Figure 6 (mixing parameters in caption). Although such a model generally reproduces the El Teniente transect trends, it requires greater amounts of crustal contaminant through time (10%–40%). Such a trend is inconsistent with at least two observations: production rates of mafic magmas that provide the heat for crustal melting decrease through time, and Sr and Nd isotope ratios that

do not correlate with silica content. The mixing model in Figure 8B, modified after Stern (1991), for Paleozoic lower crust (Sr > 1000 ppm) and basaltic magma of the southern SVZ has similar problems accounting for south to north differences in SVZ magmas.

The alternative preferred by Stern (1991) was for the crustal contaminant to enter the mantle wedge. He used the model in Figure 8B to argue that  $^{87}Sr/^{86}Sr$  ratios in magmas of the southern SVZ can be explained as 10%–20% partial melts of subarc mantle with ~1% subducted sediment contamination, whereas those ratios in the mag-

mas of the northern SVZ can be explained as 5%–10% partial melts with ~2% contamination. A similar model in Figure 8B shows that mixing variable amounts of bulk Choiyoi-like crust into the mantle wedge through forearc subduction erosion is consistent with  $^{87}Sr/^{86}Sr$  trends in El Teniente transect magmas.

As always, distinguishing crustal contaminants that enter arc magmas through MASH-like and mantle-source processes is difficult on the basis of chemistry alone. The approach used below for the El Teniente transect is to add geologic and geophysical constraints.

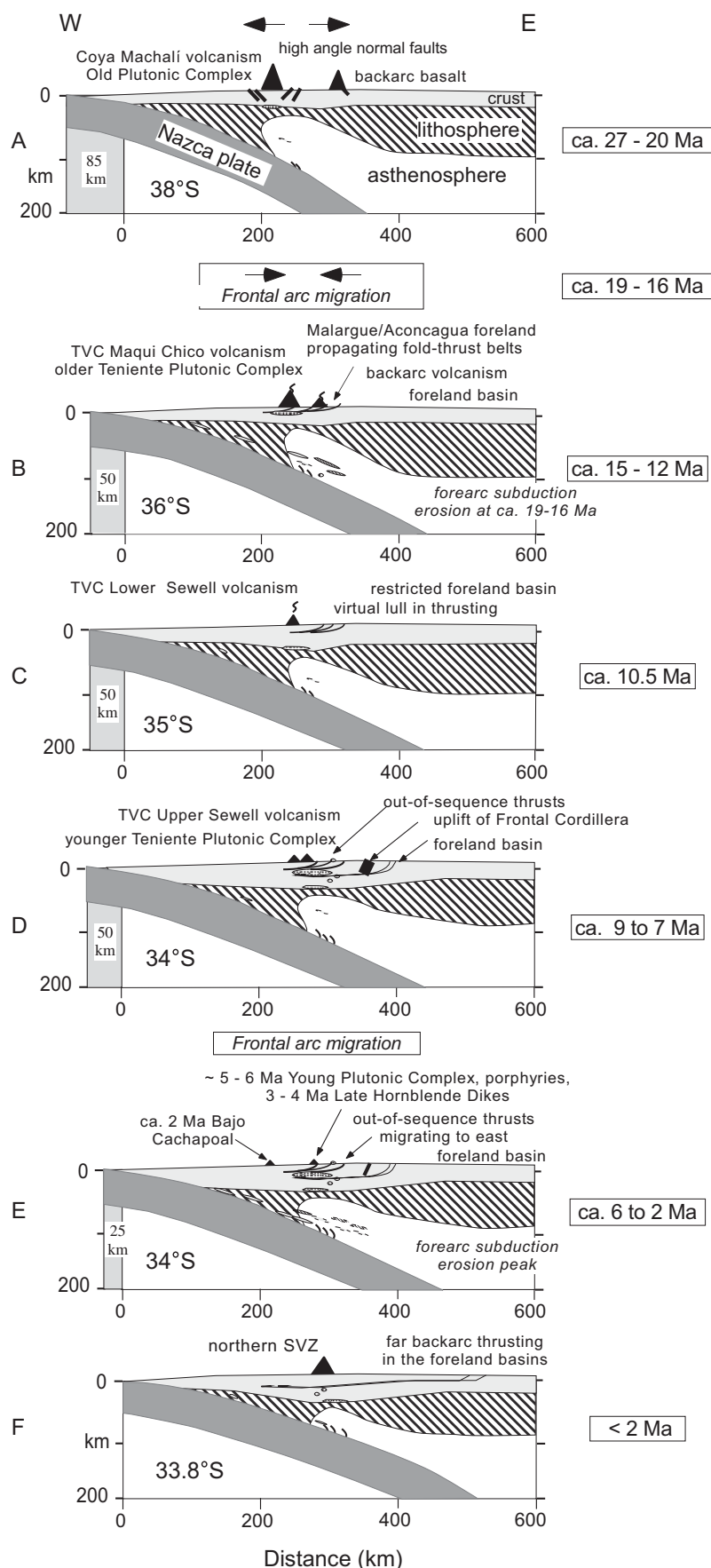


**Figure 9.** Sequence of schematic lithospheric-scale cross sections showing the early Miocene to Holocene magmatic and tectonic evolution across the El Teniente transect near 34°S. The framework of each section is based on a modern analogue along the SVZ at the latitude indicated on the section. Frontal volcanic centers (triangles) active at the time shown in the section are plotted at their present distance relative to the modern trench (km 0 on horizontal scale). Gray regions to left show the width of forearc (noted in km) added in each section to maintain an arc-trench gap like the modern one along the SVZ. Arrows indicate relative extension or contraction in backarc crust in the sections (A and B) below the arrows. Active volcanic centers, plutons, and faults are schematically shown for each time. The distributions of faults, foreland-basin sequences, and back-arc volcanic centers are based on configurations in Baldauf (1997), Godoy et al. (1999), Giambiagi et al. (2001), and Giambiagi and Ramos (2002). Fragments of crust and lithospheric mantle from the forearc are shown entering the mantle wedge under the arc at times of arc migration. Individual sections are discussed in the text.

### Lithospheric Cross Sections and the Tectonic and Magmatic History at ~34°S

Questions of mantle and crustal sources of El Teniente transect magmas are addressed below in relationship to the series of lithospheric sections in Figure 9. The frameworks of these sections are based on (1) present-day SVZ analogues according to the premise that similar magmas and structures evolve in similar settings and (2) geologic constraints from an arc to backarc transect through the El Teniente region. Crustal thicknesses in the SVZ analogues are based on gravity models in Introcaso et al. (1992), and subducting-plate geometries are from Cahill and Isacks (1992) and Pardo et al. (2002). Time slices are chosen to depict sections before and after eastward migrations of the arc front at ca. 19–16 Ma and ca. 7–3 Ma.

#### Early Miocene (ca. 27–20 Ma)

In accordance with similarities between volcanic rocks from the Coya Machali Formation the southern SVZ, the lithospheric section for the late Oligocene–early Miocene in Figure 9A is based on a SVZ transect near 38°S (Fig. 1) where the crust is ~35–40 km thick and the subducting Nazca plate is relatively steep. The shaded region near the trench represents the

~85 km of forearc crust that must be added for an ~300-km-wide arc-trench gap like that along the SVZ today to be maintained. The association of the Coya Machali Formation magmas with volcanoclastic-filled basins cut by mafic dikes fits with a transtensional stress regime (Godoy et al., 1999; Charrier et al., 2002) like that in the modern SVZ near 38°S (see Folguera and Ramos, 2000). Completing the analogy, the ca. 18.3 Ma backarc basaltic flows and breccias with intraplate-like chemical signatures near 33°30'S (Ramos et al., 1996a) are in a similar position to that of young backarc lavas near 38°S (e.g., Stern et al., 1990). The Old Plutonic Complex La Obra leucogranodiorite in the western belt of the Coya Machali Formation belt is interpreted as intruding in the waning stage of the early Miocene magmatic cycle.

This lithospheric section is consistent with the relatively low abundance, flat REE patterns in the Coya Machali Formation mafic magmas being due to either partial melting of garnet-free mantle or to high degrees of partial melting of garnet-bearing mantle leaving no residual garnet. Subsequent fractionation under low-pressure conditions is in accord with nearly parallel REE patterns that increase in level and develop larger negative Eu anomalies as SiO<sub>2</sub> increases (Fig. 4A) and with fractionating assemblages dominated by olivine, plagioclase, and pyroxene. Low <sup>87</sup>Sr/<sup>86</sup>Sr ratios and high ε<sub>Nd</sub> values (Figs. 6 and 8) fit with minimal crustal contamination in a relatively thin crust in a non-contractional stress regime.

#### *Latest Early to Middle Miocene (19–12 Ma)*

In accordance with comparisons between Teniente Volcanic Complex Maqui Chico Group lavas and SVZ lavas, the composite lithospheric section at ca. 15–12 Ma in Figure 9B is based on one in the SVZ near 36°S. The subarc crustal thickness is shown as ~40 km, and the slab dip as somewhat shallower than in the early Miocene (Fig. 9A). A change in slab dip is uncorroborated along the SVZ because of a relative lack of modern intermediate-depth slab seismicity (Cahill and Isacks, 1992). The arc front is shown ~35 km east of that in the early Miocene front in accord with regional outcrop patterns (Figs. 1 and 2). As above, the shaded region shows the width of forearc (~50 km) added to maintain a similar arc-trench gap. Overall differences with the early Miocene section require crustal thickening, frontal-arc migration, and forearc truncation.


Latest early to middle Miocene crustal thickening is a consequence of crustal shortening in the arc and backarc region. The rationale follows the Isacks (1988) model in which brittle crustal shortening in backarc Central Andean

upper crust is compensated by ductile thickening in hotter lower crust beneath the magmatic arc. Evidence for uplift accompanying such thickening comes from the accelerated exhumation (~0.55 mm/yr) rate from ca. 19–16 Ma for the La Obra pluton (Kurtz et al., 1997) that Godoy et al. (1999) linked to inversion of late Oligocene to early Miocene normal faults to the southeast of the transect. Support for additional middle Miocene thickening comes from in-sequence thrusts in the backarc Aconcagua and Malargue belts that were active from ca. 15.2 to 10.5 Ma (Giambiagi and Ramos, 2002; Baldauf et al., 1997). Increased plutonic activity from 12.3 to 11 Ma fits with facilitation of magma storage in the crust in this contractional regime.

Crustal thickening is also consistent with the steeper REE patterns in the Farellones Formation and the Maqui Chico Group samples relative to the Coya Machali Formation samples being due to higher-pressure, more amphibole-rich residual mineral assemblages equilibrating with magmas in a thicker crust (e.g., Hildreth and Moorbath, 1988; Kay et al., 1987, 1991). Lower ε<sub>Nd</sub> values and higher <sup>87</sup>Sr/<sup>86</sup>Sr ratios relative to early Miocene magmas (Figs. 6 and 8) fit with crustal contamination within the thickened crust, as well as within the mantle wedge. The somewhat higher <sup>87</sup>Sr/<sup>86</sup>Sr ratio and lower ε<sub>Nd</sub> value in the 12.3 Ma Alfalfalito pluton (Table 4) are consistent with further contamination of

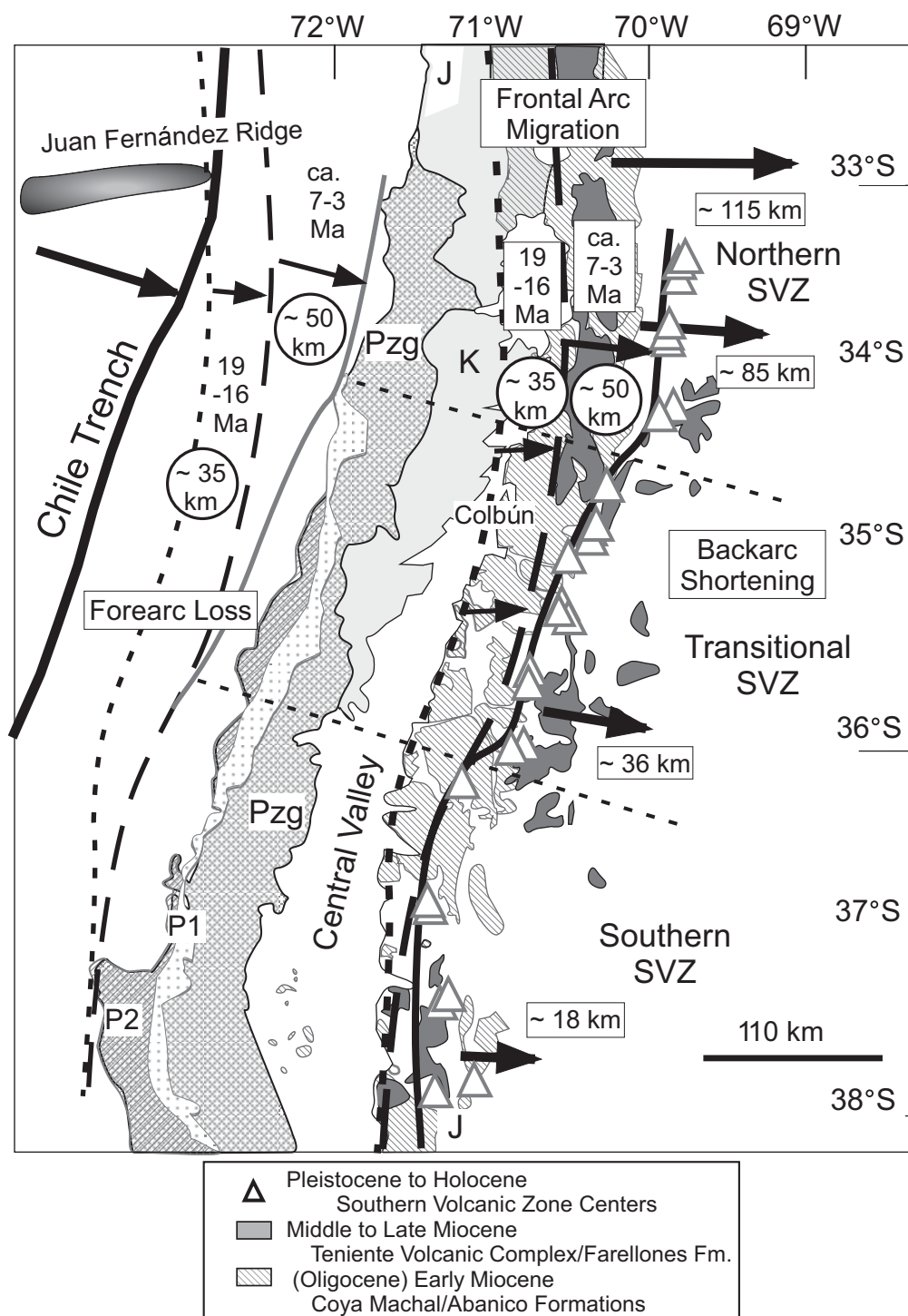
these magmas at depth within the crust. REE evidence for residual titanite in equilibrium with andesitic to rhyolitic Maqui Chico Group magmas is in accord with very oxidizing conditions beneath the reestablished arc front. Higher amphibole to clinopyroxene phenocryst ratios fit with fractionation of more hydrous, oxidized magmas at greater depth.

The hypothesis of a relatively similar arc-trench distance before and after early Miocene frontal-arc migration goes along with several lines of chemical evidence for forearc loss by subduction erosion (Fig. 9B). The first is that the Paleozoic forearc crust that would be removed (Figs. 1 and 10) is a plausible factor in the shift to higher <sup>87</sup>Sr/<sup>86</sup>Sr ratios and lower ε<sub>Nd</sub> values between the early Miocene Coya Machali Formation and the middle Miocene Teniente Volcanic Complex magmas (Figs. 6 and 8). The second is the regionally atypical high Sr concentrations (550–775 ppm) and steep REE patterns (La/Yb = 15–28; Fig. 5) in 20–18.8 Ma “adakitic” andesitic intrusions near Santiago that Yáñez et al. (2002) used as evidence for slab melting in their model for an episode of early Miocene slab break-off. Alternatively, these “adakitic” signatures could signal crustal blocks removed by subduction erosion and subjected to high-pressure metamorphism and partial melting as they were introduced into the mantle wedge (see below).



**Figure 10.** Regional map from ~32°S to 38°S as in Figure 1 with lines showing correlations of early Miocene to Holocene arc fronts on land and inferred position of corresponding coastlines offshore. Arrows show relative amounts of frontal-arc migration, forearc loss, and backarc shortening. Northwest–southeast trending dashed lines show offsets in the modern volcanic front that separate the SVZ into the northern, transitional, and southern segments. **Details:** (1) In the arc region, lines connect outcrop patterns marking early Miocene (short dashed), middle to late Miocene (long dashed), and SVZ (undashed, connecting Pleistocene to Holocene volcanic centers [triangles]) magmatic fronts. Arrows between the lines indicate inferred distance (given in circles) of frontal-arc migration from ca. 19 to 16 Ma and from ca. 7 to 3 Ma. (2) In the forearc, lines between the trench and the coast show inferred early Miocene (short dashed) and middle to late Miocene (long dashed) coastlines under the assumption that the distance of frontal-arc migration equals the width of missing coast. Former coastlines are inferred by translating the lines for the arc fronts to the west and placing the undashed line for the SVZ front near the modern coast. An underlying assumption is that the arc-trench gaps for the Miocene arcs were like that along the SVZ today. Arrows between the lines indicated inferred distance (shown in circles) of inferred loss from ca. 19 to 16 Ma. (3) In the backarc, the length and position of arrows show the location and proportional amounts of crustal shortening over the past 20 m.y. inferred from structural profiles (see Ramos et al., 2004). Shortening distances in km are: ~115 at 32°–33°S (Ramos et al., 1996b); >85 near 33.7°S (~55–60 in the Aconcagua belt, Kozłowski et al., 1993; ~24 farther east, Giambiagi and Ramos, 2002); ~36 near 36°S and ~18 near 39°S (Zapata et al., 1999). Also shown are outcrop patterns that have long been used as evidence for forearc subduction erosion along this margin. The first is the northward narrowing and disappearance of the Paleozoic high pressure (P1) and low pressure (P2) paired metamorphic and granitoid (Pzg) belts along the coast. A second is the presence of Jurassic arc rocks (marked by J) along the coast north of 33°S, but inland near the SVZ at ~38°S. K indicates Cretaceous magmatic rocks.







### **Late Miocene (10.5–7 Ma)**

The lithospheric section during Teniente Volcanic Complex Lower Sewell Group volcanism at ca. 10.5 Ma in Figure 9C and the composite section during Teniente Volcanic Complex Upper Sewell Group volcanism from ca. 9.3 to 6.5 Ma in Figure 9D are based on SVZ magmatic counterparts near 35° to 34°S where subarc crustal thicknesses are ~50–55 km. The subducting slab is again shown with a shallower dip despite a lack of substantiation by an analogue along the SVZ due to a paucity of modern slab seismicity. The arc front is shown at the same distance from the trench as in the ca. 15–12 Ma section (Fig. 9B) because there is no evidence for frontal-arc migration.

The increase in subarc crustal thickness in the ca. 10.5 Ma section (Fig. 9C) over that at ca. 15–12 Ma (Fig. 9B) fits with Lower Sewell Group magmatism postdating thin-skinned thrusting in the Aconcagua and Malargue belts (Giambiagi and Ramos, 2002; Baldauf et al., 1997). Minimal additional thickening along with a decrease in plutonism contemporaneous with Lower Sewell Group volcanism is consistent with a complementary lull in back-arc thrusting (Giambiagi et al., 2001) in a less contractional deformational regime. Evidence for renewed crustal thickening beneath the arc during Upper Sewell Group volcanism comes from a high exhumation rate in the arc region from 8 to 7 Ma (~3 mm/yr; Kurtz et al., 1997). This high rate appears linked to out-of-sequence west-dipping thrusting on the near-backarc El Fierro fault (Fig. 2; Godoy et al., 1999) and in the Aconcagua belt. Both thrust systems are related to thick-skinned thrusting during the uplift of the Frontal Cordillera (Giambiagi et al., 2001). A resumption in plutonism at this time fits with crustal magma entrapment in response to a more contractional regime. Such a situation is consistent with arc-normal compression leading to thickening of melt-weakened lower crust.

Geologic evidence for crustal thickening again correlates with trace element support for increasing amphibole to clinopyroxene ratios in residual and fractionating mineral assemblages in equilibrium with the magmas. The evidence includes higher La/Yb and Sm/Yb ratios that reflect retention of middle and, to a lesser extent, heavy REEs in residual amphibole (Figs. 4D, 4E, and 5). Crustal thickening fits with the reduction in compositional range from Teniente Volcanic Complex Maqui Chico Group (50–72% SiO<sub>2</sub>) to Lower and Upper Sewell Group (most 55%–63% SiO<sub>2</sub>) magmas being related to enhanced MASH-like processes due to longer magma residence times in a thicker crust.

Finally, relatively minor increases in <sup>87</sup>Sr/<sup>86</sup>Sr ratios and decreases in ε<sub>Nd</sub> values in ca. 15–8 Ma

Teniente Volcanic Complex magmas stand in marked contrast to larger differences between Teniente Volcanic Complex and early Miocene magmas (Figs. 6 and 8). Such a relatively small isotopic range requires little change in the type or amount of crustal contaminant as the subarc crust thickened in this period of apparent frontal-arc stability. In contrast, differences between Teniente Volcanic Complex and early Miocene magmas are consistent with crustal components' entering the mantle wedge in a peak of forearc subduction erosion during arc migration.

### **Latest Miocene–Pliocene (After 6 to ca. 2 Ma)**

The latest Miocene to Pliocene section in Figure 9E is based on a SVZ transect near ~34°S where the crust is >50 km thick. The subducting slab is shown as shallower than at ca. 8 Ma in accord with the modern Benioff zone geometry under the northern SVZ (Pardo et al., 2002). Shallowing fits with waning of magmatism in the Teniente Volcanic Complex arc as the arc broadened eastward from 7 to ca. 3 Ma, and the SVZ arc stabilized ~50 km to the east by ca. 3 Ma (Figs. 1 and 10). The shaded region near the trench shows the ~25 km of additional forearc needed to keep the arc-trench width at ~300 km at an intermediate stage of arc migration. A reduction in the partial melting percentage of a cooler garnet-bearing mantle wedge over a shallower subducting slab fits with steeper REE patterns in Pliocene Late Hornblende Dike unit mafic samples than in Miocene Teniente Volcanic Complex mafic magmas. The emplacement of the El Teniente copper deposit (see Fig. 2) is linked to magmatic processes at this time (e.g., Skewes and Stern, 1994, 1995; Kurtz et al., 1997; Kay et al., 1999; Kay and Mpodozis, 2001; Skewes et al., 2002).

The thick subarc crust in Figure 9E is in accord with ca. 6–2 Ma magmas being emplaced in the eastern part of, or just east of, the old Teniente Volcanic Complex arc after, or near the end of, out-of-sequence thrusting on the El Fierro fault and in the Aconcagua fold-thrust belt (Figs. 3, 9D). If it is assumed that the Pliocene crust was no thicker than the modern one, isostatic compensation for ~2500 m of elevation suggests an ~45–50-km-thick crust. The particularly high La/Yb and Sm/Yb ratios, small negative Eu anomalies, and high Sr contents in the Young Plutonic Complex and El Teniente porphyries then fit, at least in part, with MASH-type processes in which garnet-bearing, feldspar-poor residual assemblages equilibrated with “adakitic” magmas near the base of this thick crust. Additional support for interaction of mantle-derived mafic magmas with thickened garnet-bearing crust at high pressure comes from the flatter REE patterns in the mafic Late

Hornblende Dike unit magmas that are more closely linked to mantle sources.

The high La/Ta ratios in these magmas, like those in magmas of the northern SVZ (e.g., Hildreth and Moorbath, 1988), provide evidence for either oxide-phase retention in melt residues or relative light REE and LILE (large ion lithophile element) enrichment by fluid interaction or both. Such relative Ta depletion, like trace element evidence for titanite-bearing residual mineral assemblages in Teniente Volcanic Complex Maqui Chico Group magmas (see above), supports oxidizing and hydrous conditions in crustal magma chambers associated with the migrating or newly established magmatic front.

As at ca. 19–16 Ma, the forearc added back to the section to maintain a relatively constant arc-trench distance is consistent with a peak in subduction erosion from ca. 7 to 3 Ma (Figs. 1 and 10). Incorporation of forearc crust into the mantle wedge at this time helps to explain the coincidence of frontal-arc migration with the decrease in ε<sub>Nd</sub> values and increase in <sup>87</sup>Sr/<sup>86</sup>Sr ratios from the Miocene Teniente Volcanic Complex to the post-Pliocene magmas of the northern SVZ. Intermediate ratios in ca. 6–3 Ma lavas mark the time of arc migration (Figs. 6 and 8). Further evidence for subduction erosion could come from the very high La/Yb ratios (>40) and low Yb contents of ca. 6–5 Ma “adakitic” dacitic porphyries and leucogranodiorites (Figs. 4F and 5; see also Stern and Skewes, 1995). The problem in attributing their REE characteristics solely to a MASH process is explaining why patterns like these have not been reported in northern SVZ magmas where the crust is thicker (>50 km and possibly up to 65 km). Alternative models that call for slab melts are at odds with the Paleogene age of the subducting oceanic crust that is too old and cold to melt (Peacock et al., 1994). Like the atypical early Miocene “adakitic” magmas with high La/Yb ratios and Sr contents near Santiago, these trace element signatures fit with crustal components entering the mantle wedge in a peak of forearc subduction erosion during arc migration.

### **Latest Pliocene to Holocene (After 2.3 Ma)**

The final section at 2 Ma and later in Figure 9F is the modern transect near 34°S where subarc crustal thicknesses are ~50–55 km and the slab dip is shallower than to the south (e.g., Pardo et al., 2002). As argued by Tormey et al. (1991) among others, the steep REE patterns and radiogenic isotopic ratios of magmas of the northern SVZ fit with melts of a garnet-bearing mantle contaminated at the base of a thick arc crust. In contrast, Stern and Skewes (1995) pointed out that crustal components related to forearc

subduction erosion provide a better explanation for the chemistry of the forearc Bajo Cachapoal mafic andesites. They pointed to overlapping Sr and Nd isotope ratios in Bajo Cachapoal and northern SVZ lavas (Figs. 6 and 8) and noted that upper-crustal contaminants having low Sr contents and high  $^{87}\text{Sr}/^{86}\text{Sr}$  ratios cannot explain the high Sr (~580 ppm) contents and  $^{87}\text{Sr}/^{86}\text{Sr}$  ratios in either. Furthermore, higher  $^{87}\text{Sr}/^{86}\text{Sr}$  ratios and lower  $\epsilon_{\text{Nd}}$  values (Table 4, Fig. 8) in Bajo Cachapoal than in underlying early Miocene lavas require either more and/or different types of crustal contaminants. In contrast, these observations are easily explained if crustal components enter the magma source by subduction-erosion processes during frontal-arc migration. The isotopic similarities between northern SVZ magmas and Bajo Cachapoal magmas fit with a Choiyoi-type contaminant from the sub-forearc margin in the Bajo Cachapoal lavas and contaminants from both the thickened arc crust and subduction erosion in the northern SVZ lavas.

### Regional Correlations, Crustal Thickening, Subduction Erosion, and Magma Sources

The map in Figure 10 that shows the southern Andes from 33°S to 38°S provides a regional context in which to examine the early Miocene to Holocene processes depicted in the cross sections in Figure 9 near 34°S. Incorporated in the synthesis are mapping and chronological and geochemical results from previous investigations. Lines extending through the El Teniente transect show the first-order correlations of early Miocene (short dashed), middle to late Miocene (long dashed), and SVZ (undashed) volcanic arc fronts in this region. Starting in the west, the early Miocene front runs southward along the western edge of the Central Valley to where it goes under the SVZ south of 37°S. The chemistry of all these rocks is basically like that of the Coya Machalí Formation and magmas of the southern SVZ. Evidence for similarities along the early Miocene belt from near 33.5°S (e.g., Yáñez et al., 2002) to the Colbún region near 35.5° (e.g., La/Yb ~2–5; Vergara et al., 1999) is reviewed by Charrier et al. (2002). The similarity of early Miocene and SVZ volcanic rocks near 37°S (e.g., La/Yb ~4–10) is documented by Burns (2001). Going eastward, the middle to late Miocene magmatic front extends southward through the Teniente Volcanic Complex to where it goes under the transitional SVZ arc. The chemistry of these magmas is more variable. Those under the southern SVZ are like the early Miocene magmas (e.g., La/Yb ~4–10) as shown near 37°S by Burns (2001). Those farther north are more like Teniente Volcanic Complex–Teniente Plutonic Complex and

transitional SVZ magmas (e.g., La/Yb = 10–20), as evidenced in studies near 35°S (Baldauf, 1997) and 36°S (Nelson et al., 1999). These correlations imply that the regional chemical variations of these early Miocene to Holocene magmatic rocks reflect the same backarc, arc, and forearc events discussed above for the El Teniente transect. The processes involved are discussed below.

### Backarc Processes: Crustal Shortening and the Role of Thickened Crust

Almost all studies of SVZ magmatic rocks have stressed south to north correlations between chemical and isotopic variations and northward increases in crustal thickness. As such, a key regional observation is that estimates of post-Oligocene backarc crustal shortening based on structural profiles in Argentina and westernmost Chile are proportional to crustal thicknesses beneath the Main Andean Cordillera (Ramos et al., 1996b, 2004). These along-strike estimates are ~115 km at 32°S to 33°S, >85 km at 33.7°S, ~36 km at 36°S, and 19 km at 39°S (see Fig. 10). What is more important is that the mass-balance models based on these profiles account for crustal thicknesses beneath the Main Cordillera (Ramos et al., 1996a, 2004) without the magmatic addition called for by Nelson et al. (1999). Timing constraints on shortening between 33°S and 34.5°S (Giambiagi and Ramos, 2002) and near 35°S (Baldauf, 1997) further imply that south to north chemical variations along the SVZ and Miocene arcs, like those in the El Teniente transect reflect crustal-thickness changes linked to regional crustal-shortening events.

### Forearc Processes: Relocation of Magmatic Fronts and the Role of Subduction Erosion

A first-order observation based on the correlation of the arc fronts in Figure 10 and the El Teniente transect profiles in Figure 9 is that the magmatic arc front north of ~36.2°S moved eastward at ca. 19–16 Ma and that north of 34.8°S moved farther eastward at ca. 7–3 Ma. Given a relatively constant arc-trench gap like that west of the chemically variable SVZ today, the early Miocene trench north of 34.8°S was ~85 km farther west, that between ~34.8°S and 36.2°S was ~35 km farther west, and that south of 36.2°S was near its modern position (Fig. 10). The resulting forearc closure must be attributed to subduction erosion, westward thrusting of the former arc front into the forearc, or both.

A role for westward thrusting that puts the arc front over its forearc has appeal in explaining why the western edge of the forearc Central Valley in Figure 10 is at a nearly constant distance to SVZ centers from 37°S to 33°S, whereas the

eastern edge is ~70 km closer to the SVZ in the north. Given an early Miocene Central Valley with a width like that at 37°S today along its entire length, both its northward narrowing and the location of the Miocene arc fronts could be explained by westward thrusting over the Central Valley. Although attractive, this model has substantial problems. Most damaging is a lack of evidence for major post-early Miocene thrusts, either along the eastern part of the Central Valley or anywhere west of the early Miocene arc front. The east-dipping thrusts allowing west-directed movement that have been mapped, like the one with a décollement at 3 km that puts the western Teniente Volcanic Complex over the Coya Machalí Formation arc (Godoy et al., 1999) in Figure 2, are not of a scale to account for wholesale westward transport of these arcs. Finally, the eastward bending of the Miocene arcs in Figure 10 implies eastward migration of the arc front rather than westward tectonic transport.

On other grounds, the thrusting model provides no answer to long-term problems raised by outcrop patterns in Chile as to why the late Paleozoic metamorphic complex along the coast narrows northward and disappears near 34°S, or why the Jurassic magmatic arc, which is at the SVZ arc near 39°S, disappears northward under the Central Valley only to reemerge first along the crest of the Coastal Cordillera at 35°S and then on the coast north of 33°S (Fig. 10). Observations like these have long led to models for subduction erosion along the Chilean margin (e.g., Rutland, 1971; von Huene and Scholl, 1991; Stern, 1991) and to the proposal of Ziegler et al. (1981) that up to 250 km of the Chilean margin has been lost in the past 150 m.y. Support for active subduction erosion east of the Juan Fernández Ridge near 33°S comes from the offshore studies of von Huene et al. (1997) and Laursen et al. (2002). The latter authors argued for a long-term subduction-erosion rate of 3 km/m.y. Strong support for the subduction-erosion process in general comes from geophysical evidence for removal of large rock lenses from the forearc along the Middle American Trench (Ranero and von Huene, 2000).

Further, chemical support for a subduction-erosion component comes from the relatively abrupt shifts and transient excursions in trace element and isotopic signatures that accompanied the eastward translations of the arc front at ca. 19–16 Ma and ca. 7–3 Ma. As enumerated above, magmatic changes that accompanied these shifts include decreases in  $\epsilon_{\text{Nd}}$  values, increases in  $^{87}\text{Sr}/^{86}\text{Sr}$  ratios (Figs. 6 and 8), steeper REE patterns (higher La/Yb ratios; Fig. 5) and higher Sr contents. Such magmatic

changes require differences in the type and/or amount of crustal components and the appearance of a higher-pressure amphibole- and/or garnet-bearing, plagioclase-poor residual mineral assemblage in the magma source. As these characteristics change over a wide  $\text{SiO}_2$  range, they fit with a crustal component entering the mantle wedge. Incorporation of crust into the mantle source also best explains the isotopic and trace element “enrichment” in the ca. 2 Ma Bajo Cachapoal magmas in the SVZ forearc.

Subduction-erosion crustal components can also explain transient chemical singularities like the “adakitic” steep REE patterns and high Sr contents in the ca. 20–18.5 Ma magmatic rocks near Santiago and the ca. 6–5 Ma El Teniente transect magmatic rocks. These magmas intruded chemically distinct volcanic rocks in regions where implied crustal thicknesses are inconsistent with modeled high-pressure lower-crustal residual mineral assemblages. The preferred explanation is that these signatures reflect mantle that has been contaminated by crust removed from the forearc during episodic peaks of subduction erosion. This crust would have been subjected to high-pressure metamorphism and partially melted in the process of entering the asthenospheric mantle wedge beneath the arc (Figs. 9B and 9E). A slab-melting origin is at odds with the subduction of cold oceanic crust of Paleogene age, a temporal link with arc migration, and the observation that these “adakites,” like many proposed as slab melts based on the criteria of Defant and Drummond (1990), lack chemical and isotopic evidence for a MORB source.

Support for forearc loss and for crustal components entering the mantle wedge through subduction erosion also comes from correlating the nature of rock units cropping out along the coast with arc-migration patterns and isotopic signatures. As seen in Figure 10, coastal outcrops west of the El Teniente transect are dominantly Paleozoic plutonic rocks whereas those south of  $\sim 34.2^\circ\text{S}$  are largely Paleozoic subduction-complex metamorphic rocks in paired high- and low-pressure belts (P1 and P2 in Fig. 10, respectively) outboard of the plutonic belt. As shown by translating the geometry of the Miocene arc fronts onto the continental margin (Fig. 10), accounting for arc migration ( $\sim 35$  km at ca. 19–16 Ma,  $\sim 50$  km at ca. 7–3 Ma) by forearc subduction erosion at  $34^\circ\text{S}$  implies first removal of the Jurassic and Cretaceous forearc, then the Paleozoic metamorphic belt, and finally part of the plutonic belt. This sequence creates a parallel between increasing amounts of Choiyoi-like continental margin entering the mantle wedge through subduction erosion and the northward increases in Choiyoi-type crustal contaminants

in SVZ magmas proposed by Hildreth and Moorbath (1988). The episodic introduction of a crustal component into the mantle wedge is consistent with changes in  $^{87}\text{Sr}/^{86}\text{Sr}$  ratios and  $\epsilon_{\text{Nd}}$  values among El Teniente magmatic rocks (Figs. 6 and 8). In particular, the isotopic shift from the Miocene Teniente Volcanic Complex to the magmas of the northern SVZ coincides with  $\sim 50$  km of arc migration between ca. 7 and 3 Ma, the ratios intermediate between these in ca. 6–3 Ma Young Plutonic Complex and Late Hornblende Dike unit magmas coincide with arc migration, and the smaller shift from the early Miocene Coya Machali Formation to the Miocene Teniente Volcanic Complex magmas coincides with  $\sim 35$  km of frontal-arc migration at ca. 19–16 Ma. Episodic subduction erosion helps in rationalizing why isotopic changes in the El Teniente transect magmas correlate with episodic arc migration.

#### CONCLUSIONS: GEODYNAMIC IMPLICATIONS OF LINKS AMONG CRUSTAL SHORTENING, ARC MIGRATION, SUBDUCTION EROSION, AND MAGMATISM

The argument that crustal thickening beneath the Main Cordillera can be explained by backarc crustal shortening, whereas maintenance of a relatively constant arc-trench gap requires subduction erosion of the forearc margin, has geodynamic implications for the SVZ margin. In particular, the change in crustal width since 20 Ma needs to be the sum of backarc shortening and forearc loss. This sum is also the amount of eastward motion of the Chile Trench relative to South America east of the zone of backarc deformation. At the latitude of the El Teniente transect, the loss of continental width in the past 20 m.y. is  $\sim 170$  km:  $\sim 85$  km in the forearc due to forearc loss and  $\sim 85$  km due to backarc shortening (Fig. 10). This total is a minimum as it does not include all of the crustal shortening in Chile to the west. The magnitude of forearc loss and crustal shortening decreases to the south, reaching  $\sim 18$  km in the backarc combined with a similar forearc loss near  $38^\circ\text{S}$ .

The evidence for forearc subduction erosion as well as crustal thickening implies a significant proportion of the forearc margin must be recycled into the mantle. As calculations like that of Ramos et al. (2004) for the SVZ show that crustal thickening in the Main Andean Cordillera can be compensated in the backarc, there is little room for the lost forearc crust beneath the arc. Storage of some of this material in the forearc is one way to explain uplift and possible northward closure of the Central Valley (Fig. 10). Estimating the amount that returns

in arc magmatic rocks remains difficult as proportioning crustal contaminants in arc magmas between those entering the mantle through subduction erosion and those entering during transit through the crust remains elusive. Nevertheless, the analysis of the magmatic and tectonic framework of the SVZ region fits with contributions from subduction erosion being most significant in episodes of arc migration. Given the low magmatic production rates at these times, most of the subduction-eroded crust is not returned to the crust as a component in contemporaneous arc magmas (see also von Huene and Scholl, 1991). Some subduction-eroded crust and lithosphere may be underplated in the forearc, but most (perhaps more than 95%) may well be recycled back into the mantle.

A final observation is that estimates of forearc loss, the inferred closure of the Central Valley, frontal-arc migration, and backarc shortening are approximately the same at any given latitude between  $33^\circ\text{S}$  and  $38^\circ\text{S}$  (Fig. 10). Furthermore, the timing of major episodes of arc migration correlates with major episodes of crustal shortening. Although these correlations might be fortuitous, they seem to imply that the amount of backarc crustal shortening is dynamically linked to the amount of frontal-arc migration and forearc loss. The implication is that the whole system is being driven by eastward indentation of the continent by the relative eastward advance of the Chile Trench combined with overriding of the Nazca plate by the South American plate. The scale of these correlations shows that the Juan Fernández Ridge, which began subducting near  $33^\circ\text{S}$  at 10 Ma (Yáñez et al., 2001), can be only a minor perturbation in a much larger geodynamic scheme driven by plate interactions or mantle flow. Support for this statement comes from the correlation of the major episodes of arc migration at ca. 19–16 Ma and ca. 7–4 Ma with long recognized periods of major change along the entire Andean margin (see discussion in Kay et al., 1999; Kay and Mpodozis, 2002).

Lastly, the episodic relocations of volcanic lines, the volcanic lulls or hiatuses, and the changes in slab dip in the SVZ region speak against the concept of a “steady-state subduction zone.” The results of this study emphasize the necessity of evaluating the input and output of mass fluxes in magmatic arcs in a regional context over millions, not tens of thousands of years.

#### ACKNOWLEDGMENTS

This project was principally funded by Division El Teniente, CODELCO-Chile and FONDECYT grant 1940196. We thank R. Charrier for collaboration in sampling the Coya Machali Formation and plutons; R. Koeppen for collaboration in mapping and chemical analyses at the U.S. Geological Survey; R.W. Kay, V.A. Ramos, C. Mpodozis, and F. Camus for discus-



sion; and I. Garrido for leading Project Geodinámico El Teniente. Comments by C. Stern, M. Cloos, M. Dungan, A. Skewes, C. Miller, and L. Farmer significantly improved the manuscript. We thank CODELCO for permission to publish the results of Kay, S.M., and Kurtz, A.C., 1995, Magmatic and tectonic characterization of the El Teniente transect: Report to El Teniente Division, CODELCO-Chile, 180 p.

## REFERENCES CITED

- Aguirre, L., Féraud, G., Vergara, M., Carrasco, J., and Morata, D., 2000,  $^{40}\text{Ar}/^{39}\text{Ar}$  ages of basic flows from the Valle Nevado stratified sequence (Farellones Formation), Andes of Central Chile, in *Proceedings, IX Congreso Geológico Chileno*, Puerto Varas, Chile: Actas, v. 1, p. 583–585.
- Baldauf, P.E., 1997, Timing of the uplift of the Cordillera Principal, Mendoza Province, Argentina [Ph.D. thesis]: Washington, D.C., George Washington University, 356 p.
- Baldauf, P.E., Stephens, G.C., Nullo, F.E., Combina, A., and Kunk, M., 1997, Tertiary uplift, magmatism, and sedimentation of the Andes, southern Mendoza Province, Argentina: *Geological Society of America Abstracts with Programs*, v. 29, no. 6, p. 48.
- Beccar, I., Vergara, M., and Munizaga, F., 1986, Edades K-Ar de la Formación Farellones en el Cordon del Cerro La Parva, Cordillera de los Andes de Santiago, Chile: *Revista Geológica de Chile*, v. 28–29, p. 109–113.
- Burns, W.M., 2001, Tectonic and depositional evolution of the Tertiary Cura Mallin Basin in the southern Andes (36.5 to 38°S lat.) [Ph.D. thesis]: Ithaca, New York, Cornell University, 204 p.
- Cahill, T.A., and Isacks, B.L., 1992, Seismicity and shape of the subducted Nazca plate: *Journal of Geophysical Research*, v. 97, p. 17,503–17,529.
- Camus, F., 1975, Geology of the El Teniente ore body with emphasis on wallrock alteration: *Economic Geology*, v. 70, p. 1341–1372.
- Charrier, R., and Munizaga, F., 1979, Edades K-Ar de volcanitas cenozoicas del sector cordillerano del Río Cachapoal, Chile: *Revista Geológica de Chile*, v. 7, p. 41–51.
- Charrier, R., Wyss, A., Flynn, J., Swisher, C., III, Norell, M., Zapatta, F., McKenna, M., and Novacek, M., 1996, New evidence for late Mesozoic–early Cenozoic evolution of the Chilean Andes in the Upper Tinquirica Valley (35°S), Central Chile: *Journal of South American Earth Sciences*, v. 9, p. 393–422, doi: 10.1016/S0895-9811(96)00035-1.
- Charrier, R., Baeza, O., Elgueta, S., Flynn, J., Gans, P., Kay, S.M., Munoz, N., Wyss, A.R., and Zurita, E., 2002, Evidence for Cenozoic extensional basin development and tectonic inversion south of the flat-slab segment, southern Central Andes Chile, (33°–36°S): *Journal of South American Earth Sciences*, v. 15, p. 117–139, doi: 10.1016/S0895-9811(02)00009-3.
- Cuadra, P., 1986, Geocronología K-Ar del yacimiento El Teniente y áreas adyacentes: *Revista Geológica de Chile*, v. 27, p. 3–26.
- Defant, M.J., and Drummond, M.S., 1990, Derivation of some modern island arc magmas by melting of young subducted lithosphere: *Nature*, v. 347, p. 662–665, doi: 10.1038/347662A0.
- Dungan, M.A., Wulff, A., and Thompson, R., 2001, Eruptive stratigraphy of the Tatara–San Pedro Complex, 36°S, Southern Volcanic Zone, Chilean Andes: Reconstruction method and implications for magma evolution at long-lived arc volcanic centers: *Journal of Petrology*, v. 42, p. 555–626, doi: 10.1093/PETROLOGY/42.3.555.
- Folguera, A., and Ramos, V.A., 2000, Control estructural del volcán Copahue (38°S–71°O): Implicancias tectónicas para el arco volcánico cuaternario (36°–39°S): *Revista de la Asociación Geológica Argentina*, v. 55, p. 229–244.
- Futa, K., and Stern, C.R., 1988, Sr and Nd isotopic and trace element compositions of Quaternary volcanic centers of the southern Andes: *Earth and Planetary Science Letters*, v. 88, p. 253–263, doi: 10.1016/0012-821X(88)90082-9.
- Gana, P., Selles, D., and Wall, R., 1999, Área Ti-Til-Santiago, región Metropolitana: Santiago, Chile, Mapas Geológicos 11, SERNAGEOMIN, Subdirección Nacional de Geología y Minería, scale 1:10,000.
- Gerlach, D.C., Frey, F.A., and Moreno-Roa, H., 1988, Recent volcanics from the Puyehue-Cordon Caulle region, southern Andes, Chile (40°S): 1. Petrogenesis of evolved lavas: *Journal of Petrology*, v. 29, p. 333–382.
- Giambiagi, L.B., and Ramos, V.A., 2002, Structural evolution of the Andes in a transitional zone between flat and normal subduction (33°30′–34°S), Argentina and Chile: *Journal of South American Earth Sciences*, v. 15, p. 101–116, doi: 10.1016/S0895-9811(02)00008-1.
- Giambiagi, L.B., Tunik, M.A., and Ghiglione, M., 2001, Cenozoic tectonic evolution of the Alto Tunuyán above the transition zone between the flat and normal subduction segment (33°30′–34°S), western Argentina: *Journal of South American Earth Sciences*, v. 14, p. 707–725, doi: 10.1016/S0895-9811(01)00059-1.
- Godoy, E., 1993, Geología del Área entre Los Ríos Claro del Maipo y Cachapoal, Informe Final Proyecto Codelco-SERNAGEOMIN: Santiago, Chile, Subdirección Nacional de Geología y Minería, Open-File Report, 68 p.
- Godoy, E., Yáñez, G., and Vera, E., 1999, Inversion of an Oligocene volcano-tectonic basin and uplifting of its superimposed Miocene magmatic arc in the Central Chilean Andes: First seismic and gravity evidences: *Tectonophysics*, v. 306, p. 217–236, doi: 10.1016/S0040-1951(99)00046-3.
- Gromet, L.P., and Silver, L.T., 1987, REE variations across the Peninsular Ranges batholith: Implications for batholithic petrogenesis and crustal growth in magmatic arcs: *Journal of Petrology*, v. 28, p. 75–125.
- Hickey, R.L., Frey, F.A., Gerlach, D.C., and López-Escobar, L., 1986, Multiple sources for basaltic arc rocks from the southern volcanic zone of the Andes (34° 41'S): Trace element and isotopic evidence for contributions from subducted oceanic crust, mantle and continental crust: *Journal of Geophysical Research*, v. 91, p. 5963–5983.
- Hildreth, W., and Moorbath, S., 1988, Crustal contributions to arc magmatism in the Andes of Central Chile: Contributions to Mineralogy and Petrology, v. 98, p. 455–489.
- Introcaso, A., Pacino, M.C., and Fraga, H., 1992, Gravity, isostasy, and Andean crustal shortening between 30 and 35°S: *Tectonophysics*, v. 205, p. 31–48, doi: 10.1016/0040-1951(92)90416-4.
- Irigoyen, M.V., Buchan, K.L., and Brown, R.L., 2000, Magnetostratigraphy of Neogene Andean foreland-basin strata, lat 33 degrees S, Mendoza Province, Argentina: *Geological Society of America Bulletin*, v. 112, p. 803–816, doi: 10.1130/0016-7606(2000)112.3.CO;2.
- Isacks, B.L., 1988, Uplift of the Central Andean plateau and bending of the Bolivian orocline: *Journal of Geophysical Research*, v. 93, no. 4, p. 3211–3231.
- Kay, R.W., 1978, Aleutian magmatism: Melts from subducted Pacific Ocean crust: *Journal of Volcanological and Geothermal Research*, v. 4, p. 497–522.
- Kay, S.M., and Gordillo, C.E., 1994, Pocho volcanic rocks and the melting of depleted continental lithosphere above a shallowly dipping subduction zone in the Central Andes: Contributions to Mineralogy and Petrology, v. 117, p. 25–44.
- Kay, S.M., and Kay, R.W., 1994, Aleutian magmatism in space and time, in Plafker, G., and Berg, H.C., eds., *The geology of Alaska: Boulder, Colorado, Geological Society of America, Geology of North America*, v. G-1, p. 687–722.
- Kay, S.M., and Mpodozis, C., 2001, Central Andean ore deposits linked to evolving shallow subduction systems and thickening crust: *GSA Today*, v. 11, no. 3, p. 4–9, doi: 10.1130/1052-5173(2001)011.0.CO;2.
- Kay, S.M., and Mpodozis, C., 2002, Magmatism as a probe to the Neogene shallowing of the Nazca plate beneath the modern Chilean flat-slab: *Journal of South American Earth Sciences*, v. 15, p. 39–58, doi: 10.1016/S0895-9811(02)00005-6.
- Kay, S.M., Maksaev, V., Mpodozis, C., Moscoso, R., and Nasi, C., 1987, Probing the evolving Andean lithosphere: Middle to late Tertiary magmatic rocks in Chile over the modern zone of subhorizontal subduction (29–31.5°S): *Journal of Geophysical Research*, v. 92, p. 6173–6189.
- Kay, S.M., Kay, R.W., Citron, G.P., and Perfit, M., 1990, Calc-alkaline plutonism in the intra-oceanic Aleutian arc, Alaska, in Kay, S.M., and Rapela, C.W., eds., *Plutonism from Antarctica to Alaska: Geological Society of America Special Paper 241*, p. 233–255.
- Kay, S.M., Mpodozis, C., Ramos, V.A., and Munizaga, F., 1991, Magma source variations for mid-late Tertiary magmatic rocks associated with a shallowing subduction zone and a thickening crust in the central Andes (28 to 33°S), in Harmon, R.S., and Rapela, C.W., eds., *Andean magmatism and its tectonic setting: Geological Society of America Special Paper 265*, p. 113–137.
- Kay, S.M., Mpodozis, C., and Coira, B., 1999, Magmatism, tectonism, and mineral deposits of the Central Andes (22°–33°S latitude), in Skinner, B., ed., *Geology and ore deposits of the Central Andes: Society of Economic Geologists Special Publication 7*, p. 27–59.
- Kozlowski, E., Manceda, R., and Ramos, V.A., 1993, Estructura, in Ramos, V.A., ed., *Geología y Recursos Naturales de Mendoza, Relatorio: Mendoza, XII Congreso Geológico Argentino*, p. 149–160.
- Kurtz, A., Kay, S.M., Charrier, R., and Farrar, E., 1997, Geochronology of Miocene plutons and Andean uplift history in the El Teniente region, Central Chile (34°–35°S): *Revista Geológica de Chile*, v. 24, p. 75–90.
- Laursen, J., Scholl, D.W., and von Huene, R., 2002, Neotectonic deformation of the Central Chile margin: Deepwater forearc basin formation in response to hot spot ridge and seamount subduction: *Tectonics*, v. 21, no. 5, 1038, doi: 10.1029/2001TC901023.
- López-Escobar, L., and Vergara, M., 1997, Eocene–Miocene longitudinal depression and Quaternary volcanism in the southern Andes, Chile (33–42.5°S): A geochemical comparison: *Revista Geológica de Chile*, v. 24, p. 227–244.
- López-Escobar, L., Frey, F.A., and Vergara, M., 1977, Andesites and high-alumina basalts from the central-south Chile high Andes: Geochemical evidence bearing on their petrogenesis: Contributions to Mineralogy and Petrology, v. 63, p. 199–228.
- López-Escobar, L., Frey, F.A., and Oyarzún, J., 1979, Geochemical characteristics of Central Chile (33°–34°S) granitoids: Contributions to Mineralogy and Petrology, v. 70, p. 439–450.
- Luhr, J.F., Carmichael, I.S.E., and Varekamp, J.C., 1984, The 1982 eruptions of El Chichón volcano, Chiapas, Mexico: Mineralogy and petrology of the anhydrite-bearing pumices: *Journal of Volcanology and Geothermal Research*, v. 23, p. 69–108, doi: 10.1016/0377-0273(84)90057-X.
- Maksaev, V., Munizaga, F., McWilliams, M., Mather, R., Ruiz, J., and Fanning, M., 2003, Implications of isotope age data for the origin and evolution of the El Teniente giant porphyry Cu-Mo deposit, Chilean Andes in Proceedings, X Congreso Geológico Chileno Actas, Concepción, Chile: Extended abstracts for Symposium 2.
- Miyashiro, A., 1974, Volcanic rock series in island arcs and continental margins: *American Journal of Science*, v. 274, p. 321–355.
- Mpodozis, C., and Kay, S.M., 1992, Late Paleozoic to Triassic evolution of the Gondwana margin: Evidence from Chilean Cordilleran batholiths (28°–31°S): *Geological Society of America Bulletin*, v. 104, p. 999–1014, doi: 10.1130/0016-7606(1992)104.3.CO;2.
- Nelson, S.T., Davidson, J.P., Heizler, M.T., and Kowallis, J., 1999, Tertiary tectonic history of the southern Andes: The subvolcanic sequence to the Tatara–San Pedro volcanic complex, lat. 36°S: *Geological Society of America Bulletin*, v. 111, p. 1387–1404, doi: 10.1130/0016-7606(1999)111.3.CO;2.
- Parada, M.A., Nystrom, J.O., and Levi, B., 1999, Multiple sources for the Coastal batholith of Central Chile (31–34°S): Geochemical and Sr-Nd isotopic evidence and tectonic implications: *Lithos*, v. 46, p. 505–521, doi: 10.1016/S0024-4937(98)00080-2.
- Pardo, M., Comte, D., and Monfret, T., 2002, Seismotectonic and stress distribution in the Central Chile subduction zone: *Journal of South American Earth Sciences*, v. 15, p. 11–22, doi: 10.1016/S0895-9811(02)00003-2.
- Peacock, S.M., Rushmer, T., and Thompson, A.B., 1994, Partial melting of subducting oceanic crust: *Earth and Planetary Science Letters*, v. 121, p. 227–255, doi: 10.1016/0012-821X(94)90042-6.
- Pérez, D.J., 2000, El volcanismo neógeno de la cordillera de las Yaretas, Cordillera Frontal (34°S), Mendoza:

- Revista de la Asociación Geológica Argentina, v. 56, p. 221–239.
- Pons, D., and Vicente, J.C., 1985, Découverte d'un bois fossile de Fagaceae dans la formation Farellones (Miocène) des Andes d'Aconcagua (Chili): Importance paléobotanique et signification paléo-orographique: *Comptes Rendu de l'Académie des Sciences*, v. 110, p. 187–207.
- Price, R.C., Gray, C.M., Wilson, F.E., Frey, F.A., and Taylor, S.R., 1991, The effects of weathering on rare-earth element, Y and Ba abundances in Tertiary basalts from southeastern Australia: *Chemical Geology*, v. 93, p. 245–265, doi: 10.1016/0009-2541(91)90117-A.
- Ramos, V.A., Godoy, E., Godoy, V., and Pángaro, F., 1996a, Tectonic evolution of Main Central Andes at Paso Piuguén (33°50'S), Argentina and Chile, in *Proceedings, Third Symposium on Andean Geodynamics*, Saint-Malo, France: *Orstom/Geosciences*, p. 465–468.
- Ramos, V.A., Cegarra, M., and Cristallini, E., 1996b, Cenozoic tectonics of the High Andes of west-central Argentina (30–36°S latitude): *Tectonophysics*, v. 259, p. 185–200, doi: 10.1016/0040-1951(95)00064-X.
- Ramos, V.A., Zapata, T., and Cristallini, E.O., 2004, The Andean thrust system: Structural styles and orogenic shortening, in *McClay, K.R., ed., Thrust Tectonics and Petroleum Systems: American Association of Petroleum Geologists Memoir 82* (in press).
- Ranero, C.R., and von Huene, R., 2000, Subduction erosion along the Middle America convergent margin: *Nature*, v. 404, p. 748–752, doi: 10.1038/35008046.
- Rapp, R.P., and Watson, E.B., 1995, Dehydration melting of metabasalt at 8–32 Kbar—implication for crust-mantle recycling: *Journal of Petrology*, v. 36, p. 891–893.
- Rudnick, R.L., and Fountain, D.M., 1995, Nature and composition of the crust—a lower perspective: *Reviews of Geophysics*, v. 33, p. 267–309.
- Rutland, R.W.R., 1971, Andean orogeny and ocean floor spreading: *Nature*, v. 233, p. 252–255.
- Serrano, L., Vargas, R., Stambuk, V., Aguilar, C., Gale, M., Holmgren, C., Contreras, A., Godoy, S., Vela, I., Skewes, M.A., and Stern, C.R., 1996, The late Miocene to early Pliocene Rio Blanco–Los Bronces copper deposit, Central Chilean Andes, in *Goldfarb, R.J., and Nielsen, R.L., eds., Integrated methods for discovery: Global exploration in the 21st century: Society of Economic Geologists Special Publication 9*, p. 299–332.
- Skewes, M.A., and Holmgren, C., 1993, Solevantamiento andino, erosión y emplazamiento de brechas mineralizadas en el depósito de cobre porfídico Los Bronces, Chile Central (33°S): Aplicación de geotermometría de inclusiones fluidas: *Revista Geológica de Chile*, v. 20, p. 71–84.
- Skewes, M.A., and Stern, C.R., 1994, Tectonic trigger for formation of the late Miocene Cu-rich breccia pipes in the Andes of Central Chile: *Geology*, v. 22, p. 551–554, doi: 10.1130/0091-7613(1994)0222.3.CO:2.
- Skewes, M.A., and Stern, C.R., 1995, Genesis of the giant late Miocene to Pliocene copper deposits of Central Chile in the context of Andean magmatic and tectonic evolution: *International Geology Review*, v. 37, p. 893–909.
- Skewes, M.A., and Stern, C.R., 1996, Late Miocene mineralized breccias in the Andes of Central Chile: Sr and Nd-isotopic evidence for multiple magmatic sources, in *Camus, F., et al., eds., Andean copper deposits: New discoveries, mineralization, styles, and metallogeny: Society of Economic Geologists Special Publication 5*, p. 551–554.
- Skewes, M.A., Arévalo, A., Floody, R., Zuñiga, P.H., and Stern, C.R., 2002, The giant El Teniente breccia deposit: Hypogene copper distribution and emplacement, in *Goldfarb, R.J., and Nielsen, R.L., eds., Integrated methods for discovery: Global exploration in the 21st century: Society of Economic Geologists Special Publication 9*, p. 299–332.
- Stern, C.R., 1989, Pliocene to present migration of the volcanic front, Andean Southern Volcanic Zone: *Revista Geológica de Chile*, v. 16, p. 145–162.
- Stern, C.R., 1991, Role of subduction erosion in the generation of Andean magmas: *Geology*, v. 19, p. 78–81, doi: 10.1130/0091-7613(1991)0192.3.CO:2.
- Stern, C.R., and Skewes, M.A., 1995, Miocene to present magmatic evolution at the northern end of the Andean Southern Volcanic Zone, Central Chile: *Revista Geológica de Chile*, v. 22, p. 261–271.
- Stern, C.R., Frey, F.A., Futa, K., Zartman, R.E., Peng, Z., and Kyser, T.K., 1990, Trace element and Sr, Nd, Pb, and O isotopic composition of Pliocene and Quaternary alkali basalts of the Patagonian Plateau lavas of southernmost South America: *Contributions to Mineralogy and Petrology*, v. 104, p. 294–308.
- Sun, S.-s., and McDonough, W.F., 1989, Chemical and isotopic systematics of oceanic basalts: Implications for mantle composition and processes, in *Saunders, A.D., and Nary, M.J., eds., Magmatism in the ocean basins: Geological Society [London] Special Publication 42*, p. 313–345.
- Tormey, D.R., Hickey-Vargas, R., Frey, F.A., and López-Escobar, L., 1991, Recent lavas from the Andean volcanic front (33 to 42°S): Interpretations of along-arc compositional variations, in *Harmon, R.S., and Rapela, C.W., eds., Andean magmatism and its tectonic setting: Geological Society of America Special Paper 265*, p. 57–78.
- Tormey, D.R., Frey, F., and López-Escobar, L., 1995, Geochemistry of the active Azufre-Plancho-Peteroa volcanic complex, Chile (35°15'S): Evidence for multiple sources and processes in a Cordilleran arc magmatic system: *Journal of Petrology*, v. 36, p. 265–298.
- Vergara, M., Charrier, R., Munizaga, F., Rivano, S., Sepúlveda, P., Thiele, R., and Drake, R., 1988, Miocene volcanism in the Central Chilean Andes (31°30'–34°35'S): *Journal of South American Earth Sciences*, v. 1, p. 199–209, doi: 10.1016/0895-9811(88)90038-7.
- Vergara, M., Morato, D., Hickey-Vargas, R., López-Escobar, L., and Becar, I., 1999, Cenozoic tholeiitic volcanism in the Colburn area, Linares Precordillera, Central Chile: *Revista Geológica de Chile*, v. 26, p. 23–41.
- von Huene, R., and Scholl, D.W., 1991, Observations at convergent margins concerning sediment subduction, subduction erosion, and the growth of continental crust: *Reviews of Geophysics*, v. 29, p. 279–316.
- von Huene, R., Corvalán, J., Fleuh, E.R., Hinz, K., Korstgard, J., Ranero, C.R., Weinrebe, W., and Condor Scientists, 1997, Tectonic control of the subducting Juan Fernández Ridge on the Andean margin near Valparaíso, Chile: *Tectonics*, v. 16, p. 474–488.
- Warnaars, F.W., Holmgren, C., and Brassy, S., 1985, Porphyry copper and tourmaline breccias at Los Bronces–Rio Blanco, Chile: *Economic Geology*, v. 80, p. 1544–1565.
- Yáñez, G.A., Ramiro, C., von Huene, R., and Diaz, J., 2001, Magnetic anomaly interpretation across the southern central Andes (32°–34°S): The role of the Juan Fernández Ridge in the late Tertiary evolution of the margin: *Journal of Geophysical Research*, v. 106, p. 6325–6345, doi: 10.1029/2000JB900337.
- Yáñez, G.A., Cembrano, J., Pardo, N., Ranero, C., and Selles, D., 2002, The Challenger–Juan Fernández–Maipo major tectonic transition of the Nazca–Andean subduction system at 33°–34°S: Geodynamic evidence and implications: *Journal of South American Earth Sciences*, v. 15, p. 23–38, doi: 10.1016/S0895-9811(02)00004-4.
- Zapata, T.I., Brissón, I., and Dzelalija, F., 1999, The structures of the Andean fold and thrust belt in relation to basement control in the Neuquén Basin: *Boletín de Informaciones Petroleras*, v. 16, p. 112–121.
- Ziegler, A.M., Barrett, S.F., and Scotese, C.R., 1981, Paleoclimate, sedimentation, and continental accretion: *Philosophical Transactions of the Royal Society London, Series A*, v. 301, p. 253–264.

MANUSCRIPT RECEIVED BY THE SOCIETY 27 JUNE 2003

REVISED MANUSCRIPT RECEIVED 4 FEBRUARY 2004

MANUSCRIPT ACCEPTED 1 MARCH 2004

Printed in the USA